Modeling of the cyclic behavior of elastic–viscoplastic composites by the additive tangent Mori–Tanaka approach and validation by finite element calculations

C. Czarnota [a], K. Kowalczyk-Gajewska [b,*], A. Salahouelhadj [a], M. Martiny [a], S. Mercier [a]

[a] Laboratoire d'Etude des Microstructures et de Mécanique des Matériaux, LEM3 – UMR CNRS 7239, Université de Lorraine, Île du Saulcy, 57045 METZ Cedex 1, France
[b] Institute of Fundamental Technological Research (IPPT PAN), Pawińskiego 5B, 02-106 Warsaw, Poland

ABSTRACT

This work deals with the prediction of the macroscopic behavior of two-phase composites, based on the Mori–Tanaka scheme combined with an additive/sequential interaction rule and tangent linearization of viscoplastic response. Cyclic tension compression loadings are considered to further validate the approach. The composite is made of spherical inclusions dispersed in a matrix. Both materials have an elastic–viscoplastic behavior. In a second part, finite element calculations are performed using ABAQUS/STANDARD software in order to validate the proposed homogenization technique. A representative volume element is analyzed with 30 randomly distributed inclusions. Comparisons between the additive tangent Mori–Tanaka scheme and finite element calculations are made for different volume fractions of inclusions, different contrasts in elastic and viscous properties and different strain rates and strain amplitudes. These comparisons demonstrate the efficiency of the proposed homogenization scheme. The effect of isotropization of the viscoplastic tangent stiffness is also investigated. It is concluded that quality of predictions does not benefit from such simplification, contrary to the known result for elastic–plastic case.

© 2014 Elsevier Ltd. All rights reserved.

1. Introduction

The problem of finding the overall response of heterogeneous elastic–viscoplastic material is addressed in the present paper. The local constitutive relation for the material phases in the following is of Maxwell-type form:

$$\dot{\boldsymbol{\varepsilon}} = \dot{\boldsymbol{\varepsilon}}_e + \dot{\boldsymbol{\varepsilon}}_v = \mathbb{M}_e \cdot \dot{\boldsymbol{\sigma}} + f(\boldsymbol{\sigma}), \qquad (1)$$

where $\dot{\boldsymbol{\varepsilon}}$ is a strain rate tensor, $\dot{\boldsymbol{\varepsilon}}_e$ and $\dot{\boldsymbol{\varepsilon}}_v$ are its elastic and viscoplastic parts, $\boldsymbol{\sigma}$ is the stress tensor, $\dot{\boldsymbol{\sigma}}$ its time derivative and $\mathbb{M}_e$ is the fourth order tensor of elastic compliance. Different expressions of the nonlinear function $f(\boldsymbol{\sigma})$ specifying the dependence of viscous strain rate on the stress are available and will be analyzed below. The attention will be focused on the two-phase metal-matrix composites.

Most of the mean-field methods dedicated to the estimation of effective properties of heterogenous media originate in Eshelby's solution for the ellipsoidal inclusion problem when an inhomogeneity is embedded into an infinite linearly elastic matrix (Eshelby, 1957). The main outcome of this solution is the fact that the strain

inside the inclusion $\boldsymbol{\varepsilon}_i$ is uniform and related to the far-field strain $\boldsymbol{\varepsilon}_0$ by the fourth order Eshelby tensor. In 1965, Hill noticed an important consequence of this result written in the form of the so-called interaction equation:

$$\boldsymbol{\sigma}_i - \boldsymbol{\sigma}_0 = -\mathbb{L}_* \cdot (\boldsymbol{\varepsilon}_i - \boldsymbol{\varepsilon}_0), \qquad (2)$$

in which $\boldsymbol{\sigma}_i$ and $\boldsymbol{\sigma}_0$ are correspondingly the stress tensor in the inclusion and the far-field stress tensor, while the fourth order tensor $\mathbb{L}_*$ is the Hill tensor that is calculated with use of the Green function for the reference elastic medium. It depends on the reference elastic stiffness $\mathbb{L}_0$ and the shape of inclusion. The whole derivations of relation (2) remain valid as long as the constitutive law stays linear or affine and relates the stress or stress rate with strain or strain rate, as for example in linear viscosity or linear elasticity.

The interaction equation proves to be very useful in formulating different micro–macro transition schemes developed for estimating the effective properties of heterogeneous materials. One can cite:

- the Mori–Tanaka scheme (1973) applied widely for particulate composites where $\boldsymbol{\varepsilon}_0 = \bar{\boldsymbol{\varepsilon}}_m$ and $\boldsymbol{\sigma}_0 = \bar{\boldsymbol{\sigma}}_m$ are an average strain and an average stress in the matrix, while the reference stiffness $\mathbb{L}_0$ is the matrix stiffness $\mathbb{L}_0 = \mathbb{L}_m$;

- the self-consistent scheme (Kröner, 1958; Hill, 1965) usually applied for polycrystalline materials. When all grains have the same shape and orientation, one has: $\boldsymbol{\varepsilon}_0 = \bar{\boldsymbol{\varepsilon}}$ and $\boldsymbol{\sigma}_0 = \bar{\boldsymbol{\sigma}}$ where $\bar{\boldsymbol{\varepsilon}}$ (resp. $\bar{\boldsymbol{\sigma}}$) is an average strain (resp. an average stress) in the polycrystalline representative volume (aggregate). The reference stiffness tensor $\mathbb{L}_0$ refers to the unknown homogenized properties of the aggregate, $\bar{\mathbb{L}}$.

The relation (2) is also very efficient when formulating the generalization of those two schemes for non-linear constitutive behavior. In the case of elasto-plasticity or non-linear viscoplasticity, linearization of response is performed (Hill, 1965; Hutchinson, 1976; Berveiller and Zaoui, 1979; Molinari et al., 1987; Lebensohn and Tomé, 1993; Kiryk and Petryk, 1998; Masson et al., 2000). Depending on the linearization method, the stiffness tensor $\mathbb{L}_0$ can be interpreted as tangent or secant stiffness.

The procedure complicates in the case of elastic–viscoplastic materials because stress and stress rate appear in the constitutive relation at the same time, especially when the viscous and elastic parts of the strain rate are of comparable magnitude and none of them can be neglected as schematically depicted in Fig. 1. When linear viscosity is considered, standard methodology involving Laplace transform (LT) technique and the correspondence principle can be applied (Hashin, 1969; Christensen, 1969; Laws and McLaughlin, 1978; Suquet, 1985; Rougier et al., 1993; Rougier et al., 1994; Turner and Tomé, 1994; Li and Weng, 1994; Brinson and Lin, 1998; De Botton and Tevet-Deree, 2004; Pichler and Lackner, 2009; Brenner and Suquet, 2013). The interaction relation (2) is then recovered, although, it is formulated in the Laplace space, namely

$$\hat{\boldsymbol{\sigma}}_i(s) - \hat{\boldsymbol{\sigma}}_0(s) = -\hat{\mathbb{L}}_*(s) \cdot (\hat{\boldsymbol{\varepsilon}}_i(s) - \hat{\boldsymbol{\varepsilon}}_0(s)), \tag{3}$$

where $\hat{(.)}$ refers to the Laplace transform of $(.)$ and s in Eq. (3) represents the Laplace variable. In order to find actual solution in the real space, an inverse Laplace transform is required. This technique gives exact solution only for non-ageing linear visco elastic behavior. In the case of non-linear viscosity the Laplace technique is not straightforward (Rougier et al., 1994; Masson and Zaoui, 1999; Pierard and Doghri, 2006; Pierard et al., 2007; Ricaud and Masson, 2009). The inverse Laplace transform (performed numerically) may lead to approximations which are difficult to quantify.

Therefore, approximate methods in which the form of the interaction equation is postulated in the real time space are of interest to reproduce the actual solution in a way as accurate as possible.
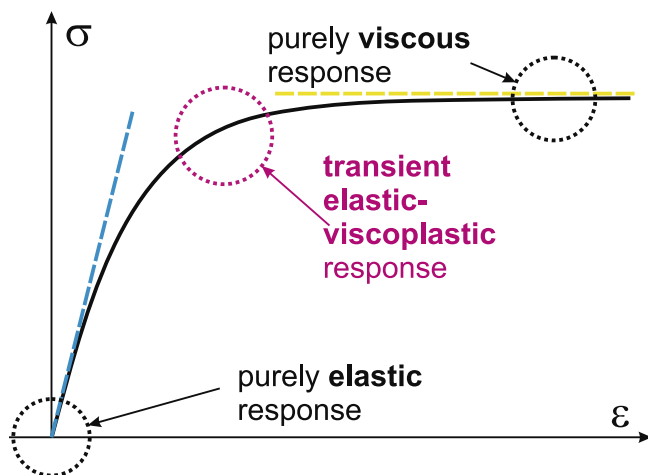

Fig. 1. Typical uniaxial stress–strain response for elastic–viscoplastic material deformed at constant strain rate.

One of such proposals is the additive interaction rule due to Molinari (2002), see also (Kouddane et al., 1993; Molinari et al., 1997; Mercier and Molinari, 2009). Since the strain rate can be decomposed additively into elastic and plastic parts (Eq. 1) and since well established and validated interaction laws exist for each of these parts separately, the following form has been proposed:

$$\dot{\boldsymbol{\varepsilon}}_i - \dot{\boldsymbol{\varepsilon}}_0 = -\mathbb{M}_*^v \cdot (\boldsymbol{\sigma}_i - \boldsymbol{\sigma}_0) - \mathbb{M}_*^e \cdot (\dot{\boldsymbol{\sigma}}_i - \dot{\boldsymbol{\sigma}}_0), \tag{4}$$

where $\mathbb{M}_*^v$ and $\mathbb{M}_*^e$ are the inverse Hill tensors obtained with use of the tangent viscoplastic and elastic stiffnesses. The tangent viscous stiffness is defined by performing the following linearization of local relation:

$$\dot{\boldsymbol{\varepsilon}}_v = f(\boldsymbol{\sigma}) = \mathbb{M}^{v(tan)} \cdot \boldsymbol{\sigma} + \dot{\boldsymbol{\varepsilon}}_v^{res}, \tag{5}$$

where the inverse tangent moduli $\mathbb{M}^{v(tan)}$ are uniquely specified as

$$\mathbb{M}^{v(tan)} = \frac{\partial f(\boldsymbol{\sigma})}{\partial \boldsymbol{\sigma}}, \tag{6}$$

and $\dot{\boldsymbol{\varepsilon}}_v^{res} = f(\boldsymbol{\sigma}) - \mathbb{M}^{v(tan)} \cdot \boldsymbol{\sigma}$ is a back extrapolated strain. A secant approach with $\mathbb{M}^{v(sec)}$ (where $\dot{\boldsymbol{\varepsilon}}_v = \mathbb{M}^{v(sec)} \cdot \boldsymbol{\sigma}$) could be also proposed but the definition of the secant stiffness is not unique (Molinari et al., 1997). In addition, most of the studies of the literature indicate that the tangent linearization of the viscoplastic behavior provides more reliable predictions (Molinari and Toth, 1994; Molinari et al., 2004; Lebensohn et al., 2004). The interaction law (4), employing tangent viscous compliance, was first successfully validated based on finite element calculations when considering the problem of an ellipsoidal inclusion embedded into an infinite matrix (Mercier et al., 2005) and subsequently compared with other models and finite element calculations for estimating the effective properties of the composite (Mercier and Molinari, 2009; Mercier et al., 2012).

In (Kowalczyk-Gajewska and Petryk, 2011) a related but conceptually different approach was formulated. The idea of incorporating both elastic and viscoplastic properties in a single computational step of incremental analysis of the inhomogeneity problem was abandoned. As an alternative, sequential linearization was proposed. Consequently, a sequence of interaction equations is postulated in place of a single interaction equation. For elastic/viscous materials, two relations are considered:

$$\dot{\boldsymbol{\varepsilon}}_i^v - \dot{\boldsymbol{\varepsilon}}_0^V = -\mathbb{M}_*^v \cdot (\boldsymbol{\sigma}_i - \boldsymbol{\sigma}_0^V), \tag{7}$$

$$\dot{\boldsymbol{\varepsilon}}_i^e - \dot{\boldsymbol{\varepsilon}}_0^E = -\mathbb{M}_*^e \cdot (\dot{\boldsymbol{\sigma}}_i - \dot{\boldsymbol{\sigma}}_0^E), \tag{8}$$

where kinematic consistency is additionally imposed, i.e. $\dot{\boldsymbol{\varepsilon}}_0^V + \dot{\boldsymbol{\varepsilon}}_0^E = \dot{\boldsymbol{\varepsilon}}_0$. Different variants of the method were analyzed by varying definitions of the auxiliary variables $\dot{\boldsymbol{\varepsilon}}_0^V, \dot{\boldsymbol{\varepsilon}}_0^E, \boldsymbol{\sigma}_0^V, \dot{\boldsymbol{\sigma}}_0^E$. The variant in which $\boldsymbol{\sigma}_0^V = \boldsymbol{\sigma}_0$ and $\dot{\boldsymbol{\sigma}}_0^E = \dot{\boldsymbol{\sigma}}_0$ proved to produce the best results when compared to the exact solution for compressible linear viscoelastic materials. It can be easily noticed that for this variant, the sequential linearization method and the additive interaction rule (4) are equivalent. Consideration of two subproblems (elastic and viscous ones) could be interpreted as a subdivision of the loading step into a creep-type process during which the stress level (denoted V in Fig. 2) is kept constant and an instantaneous elastic process (denoted E).

Other approximate schemes for elastic–viscoplastic materials can originate from the translated field (TF) method (Paquin et al., 1999; Sabar et al., 2002; Berbenni et al., 2004; Mareau and Berbenni, 2015). Instead of formulating the theory with an interaction law, the localization equation, relating strain in the inhomogeneity to a far field strain, is constructed. Comparison between additive interaction law and TF method predictions are available in (Mercier et al., 2012).
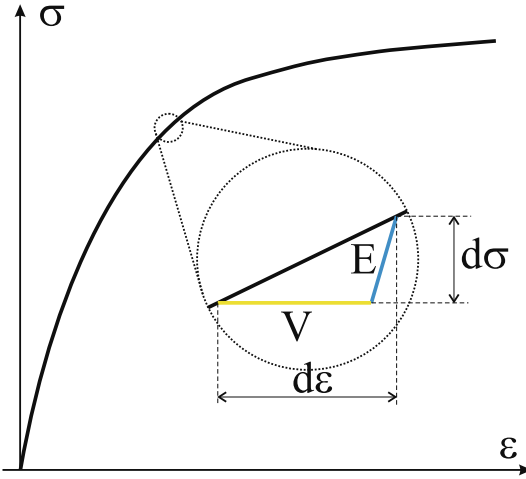
Fig. 2. Decomposition of the incremental elastic–viscoplastic response into a creep-type step (labeled (V)) and an instantaneous elastic step (labeled (E)).

Additional works were recently developed to tackle the elastic–viscoplastic case and can be found in the literature, see for instance (Coulibaly and Sabar, 2011). There are also variational formulations (Lahellec and Suquet, 2007; Doghri et al., 2010; Lahellec and Suquet, 2013), some of them enable to account for second order heterogeneities in a way similar to the methodology developed for non-linear viscous composites by Ponte Castañeda (1992). The main difficulties in those models are to formulate the rate potential for the linear comparison composite and to perform, at each time increment, the minimization procedure to find the optimal solution. A large series of papers proved its accuracy for various types of material properties.

In elasto-viscoplasticity, the formulation of the Mori–Tanaka scheme based on the additive interaction law or, equivalently, on sequential interaction rules proceeds as smoothly as for linear elasticity: $\dot{\boldsymbol{\varepsilon}}_0, \boldsymbol{\sigma}_0$ and $\dot{\boldsymbol{\sigma}}_0$ are replaced by the corresponding average fields in the matrix: $\dot{\bar{\boldsymbol{\varepsilon}}}_m, \bar{\boldsymbol{\sigma}}_m$ and $\dot{\bar{\boldsymbol{\sigma}}}_m$, while $\mathbb{L}_0^e = \mathbb{L}_m^e$ and $\mathbb{L}_0^v = \mathbb{L}_m^v$ are elastic and viscous (tangent) stiffness tensors of the matrix.

Similarly, the additive interaction equation can be used to formulate the self-consistent scheme: $\dot{\boldsymbol{\varepsilon}}_0, \boldsymbol{\sigma}_0$ and $\dot{\boldsymbol{\sigma}}_0$ are now replaced by the corresponding average overall fields: $\dot{\bar{\boldsymbol{\varepsilon}}}, \bar{\boldsymbol{\sigma}}$ and $\dot{\bar{\boldsymbol{\sigma}}}$, while $\mathbb{L}_0^e = \bar{\mathbb{L}}^e$ and $\mathbb{L}_0^v = \bar{\mathbb{L}}^v$ are the homogenized elastic and viscous (tangent) stiffnesses obtained as solutions of purely elastic and purely viscous problems, respectively. The additive interaction rule in the conjunction with the self-consistent averaging scheme was adopted by Wang et al. (2010) to model the cyclic response of polycrystalline materials within the large strain framework. Let us remark that in the literature concerning polycrystalline materials (Molinari et al., 1997; Masson et al., 2000; Bornert et al., 2001) there exist different approaches based on the tangent linearization proposed by Molinari et al. (1987) and leading to the so-called tangent and affine schemes. In both approaches, the local linearization of the material behavior is identical. A difference in overall predictions originates from the different constitutive behavior selected for the reference medium. For the Mori–Tanaka approach, the reference medium is the matrix phase, so there is no difference between affine and tangent modeling.

As concerns the sequential approach, an equivalent relation would be obtained for the same choice of homogenized elastic and viscous stiffnesses and assuming the following kinematic consistency relation $\dot{\boldsymbol{\varepsilon}}_0^V + \dot{\boldsymbol{\varepsilon}}_0^E = \dot{\bar{\boldsymbol{\varepsilon}}}$ and $\boldsymbol{\sigma}_0^V = \bar{\boldsymbol{\sigma}}$ and $\dot{\boldsymbol{\sigma}}_0^E = \dot{\bar{\boldsymbol{\sigma}}}$. However, it has been shown in (Kowalczyk-Gajewska and Petryk, 2011) that more satisfactory estimates, at least for moderate non-linearity, are obtained when an additional accommodation subproblem is solved.

In this paper we focus on the Mori–Tanaka scheme employing the tangent linearization of viscoplastic relation. Therefore both approaches (additive interaction law or sequential interaction rule) coincide. In the following, the proposed scheme will be named the additive tangent Mori–Tanaka approach. When estimating overall elastic–viscoplastic response with mean field approaches, two types of approximations are introduced. Firstly, we approximate the solution of the Eshelby problem by introducing the additive tangent interaction rule. Secondly the Mori–Tanaka scheme is used to estimate the overall response of the composite. Finite element calculations enable verification of both approximations. The first step has been successfully validated by Mercier et al. (2005). As concerns the second stage, for validation purposes, proportional processes of uniaxial tension/compression or plane strain compression have been considered in the case of non-linear viscosity e.g. by: Mercier and Molinari (2009); Kowalczyk-Gajewska and Petryk (2011); Mercier et al. (2012). Tension–compression cycles were considered for the linear viscosity case in (Kowalczyk-Gajewska and Petryk, 2011) or for the non-linear elastic–viscoplastic case but with quite large value of the strain rate sensitivity in (Mercier and Molinari, 2009; Mercier et al., 2012). In previous papers, validation has focused on the proper assessment of the composite overall response. However, multiscale approaches can be also applied to find the local average response per phases. Therefore, in the present paper, in order to validate the proposed approach also in the latter respect, Finite Element calculations on a 3D Representative Volume Element (RVE) are performed. Based on the numerical simulations, the overall behavior, the average local behavior per phases and, additionally, the intra-phase heterogeneity can be studied. Verification of model predictions for deformation processes involving strain path changes such as multiple tension–compression cycles, is performed. When considering cyclic tension–compression, transient elastic–viscoplastic regimes (Fig. 1) occur many times. As a consequence, such a combined approach based on analytical and numerical analyzes provides insight into proving the good capability of the analytical model. The effect of isotropization of some tensors involved in the definition of the viscoplastic Hill tensor $\mathbb{L}_*^v$ has also been investigated. Contrary to the case of elasto-plasticity, it is observed that the predictions of the composite response based on the Mori–Tanaka model with use of an additive tangent interaction law, do not benefit from such isotropization.

In the examples we concentrate on elastic–viscoplastic materials, with non-linear viscous properties and low strain rate sensitivity value. So the present contribution concerns mostly metal-matrix composites.

2. The additive tangent Mori–Tanaka scheme

In the present paper, we consider a two-phase composite material. The phases have non-linear elastic–viscoplastic behavior. Fig. 3 presents a schematic view of the composite made of spherical inclusions embedded into the matrix. The volume fraction of inclusions is denoted by c. Subscript i (resp. m) refers to the inclusion (resp. matrix) phase. The composite material is subjected to a macroscopic strain rate tensor $\dot{\bar{\boldsymbol{\varepsilon}}}$ prescribed at the remote boundary of the RVE. The total strain rate in each phase is decomposed into elastic and viscous parts:

$$\dot{\boldsymbol{\varepsilon}} = \dot{\boldsymbol{\varepsilon}}^e + \dot{\boldsymbol{\varepsilon}}^v. \tag{9}$$

The elastic strain rate $\dot{\boldsymbol{\varepsilon}}^e$ is linked to the Cauchy stress rate tensor $\dot{\boldsymbol{\sigma}}$ by the incremental elastic law:

$$\dot{\boldsymbol{\varepsilon}}^e = \mathbb{M}^e \cdot \dot{\boldsymbol{\sigma}}, \tag{10}$$

where $\mathbb{M}^e$ is the fourth order tensor of elastic compliance and the operator $(\cdot)$ is the double contracted product. The present contribution is restricted to a small deformation theory.
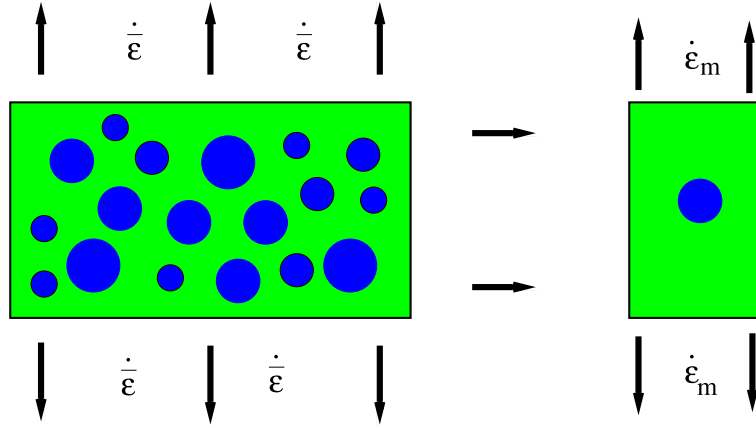
Fig. 3. Schematic representation of the composite. Spherical inclusions are dispersed in the matrix phase, the volume content of inclusion phase is c. The composite material is subjected to a macroscopic strain rate tensor $\dot{\bar{\varepsilon}}$ prescribed at the remote boundary. The inclusion problem for the Mori–Tanaka scheme is represented by an inclusion embedded in an infinite volume, made of matrix phase, subjected to the average matrix strain rate tensor $\dot{\boldsymbol{\varepsilon}}_m$.

Two constitutive laws accounting for viscoplasticity are analyzed. In the first approach the equivalent viscous strain rate $\dot{\varepsilon}^{eq} \equiv \sqrt{2/3 \dot{\boldsymbol{\varepsilon}}^v \cdot \dot{\boldsymbol{\varepsilon}}^v}$ is connected with the equivalent Huber-von Mises stress $\sigma^{eq} \equiv \sqrt{3/2 \mathbf{s} \cdot \mathbf{s}}$ by a power-law relation

$$\sigma^{eq} = \sigma_Y \left(\frac{\dot{\varepsilon}^{eq}}{\dot{\varepsilon}_o} \right)^m, \tag{11}$$

where m is the strain rate-sensitivity parameter, $\dot{\varepsilon}_o$ is a reference strain rate, σ_Y is a reference flow stress corresponding to the flow stress when $\dot{\varepsilon}^{eq} = \dot{\varepsilon}_o$ and $\mathbf{s}$ represents the deviator of the Cauchy stress tensor. The viscoplastic flow rule has the form:

$$\dot{\boldsymbol{\varepsilon}}^v = \dot{\varepsilon}^{eq} \frac{3\mathbf{s}}{2\sigma^{eq}}. \tag{12}$$

In the second approach, the Perzyna-type viscoplasticity model with an over-stress function Φ is considered (Perzyna, 1986):

$$\dot{\boldsymbol{\varepsilon}}^v = \Phi \frac{\partial f}{\partial \boldsymbol{\sigma}} = \Phi \frac{3\mathbf{s}}{2\sigma^{eq}}, \tag{13}$$

where

$$f = \sigma^{eq} - \sigma_Y - R(\varepsilon^{eq}), \quad \Phi = \begin{cases} \dot{\varepsilon}_o \left(\frac{f}{\sigma_Y + R(\varepsilon^{eq})} \right)^{\frac{1}{m}} & \text{if } f > 0, \\ 0 & \text{otherwise}. \end{cases} \tag{14}$$

For this model, the viscous flow is initiated when the function f is positive. Parameters m and $\dot{\varepsilon}_o$ have similar meaning as for the power law, σ_Y is now an initial flow stress (no plastic pre-strain) under static conditions. The function $R(\varepsilon^{eq})$ is non-linear and describes the hardening behavior of different phases:

$$R(\varepsilon^{eq}) = k(\varepsilon^{eq})^n. \tag{15}$$

Quantities k and n are additional material parameters. From Eqs. (13)–(15), the Perzyna model can be rewritten in the following form (valid after initiation of the viscous flow):

$$\sigma^{eq} = \left(\sigma_Y + k(\varepsilon^{eq})^n \right) \left(1 + \left(\frac{\dot{\varepsilon}^{eq}}{\dot{\varepsilon}_o} \right)^m \right). \tag{16}$$

Since we focus on the modeling of composite reinforced by spherical inclusions, the additive tangent Mori–Tanaka scheme based on (Mercier and Molinari, 2009) is adopted. The average strain rate $\dot{\boldsymbol{\varepsilon}}_i$ in the inclusion is linked to the average strain rate $\dot{\boldsymbol{\varepsilon}}_m$ in the matrix, see Fig. 3, by the additive interaction equation:

$$\dot{\boldsymbol{\varepsilon}}_i - \dot{\boldsymbol{\varepsilon}}_m = -\mathbb{M}_*^v \cdot (\boldsymbol{\sigma}_i - \boldsymbol{\sigma}_m) - \mathbb{M}_*^e \cdot (\dot{\boldsymbol{\sigma}}_i - \dot{\boldsymbol{\sigma}}_m), \tag{17}$$

where $\boldsymbol{\sigma}_m$ (resp. $\boldsymbol{\sigma}_i$) represents the average Cauchy stress tensor in the matrix (resp. in the inclusion). In the case of non-linear viscosity the Hill tensor $\mathbb{M}_*^v$ is calculated using the average stress in the matrix $\boldsymbol{\sigma}_m$ and the tangent viscoplastic stiffness of the matrix phase.

The additive interaction law, in addition to its simple mathematical structure, has other advantages. Firstly, the valid solutions for purely elastic and purely viscous materials are obtained as limit cases. Secondly, for isotropic incompressible linear viscoelastic materials, the exact solution of the inclusion problem due to Hashin (1969) is recovered. In addition the elastic and viscoplastic behaviors of the phases can be compressible or incompressible. All these assets are also shared by all the variants of the sequential linearization method. The validity of the proposed approximation in the presence of elastic compressibility has been studied in (Mercier et al., 2005 and Kowalczyk-Gajewska and Petryk, 2011). By comparison with exact solution obtained based on the Laplace transform or based on finite element calculations, it was found that differences are not significant and the approximated interaction law remains valid in this case. For metallic materials, viscoplasticity is usually incompressible, thus most of the applications have been considering such an assumption. It is also the case for relations (12) and (13). Nevertheless, the validity of Eq. (4) has been also checked for dilatant inelastic materials, see (Mercier et al., 2012). In view of these studies, the proposed additive interaction law can be used for general viscoplastic behaviors. For example it could be also adopted for porous metallic matrix. This has not yet been considered but could be done in the future.

From the interaction law (17), the incremental elastic law (10) for inclusion and matrix phases and for incompressible viscoplasticity, the average strain rate in the inclusion is given by:

$$\dot{\boldsymbol{\varepsilon}}_i = \left(\mathbb{M}_i^{e^{-1}} + \mathbb{M}_*^{e^{-1}} \right)^{-1} \cdot \left[\mathbb{M}_i^{e^{-1}} \cdot \dot{\boldsymbol{\varepsilon}}_i^v + \mathbb{M}_m^{e^{-1}} \cdot (\dot{\boldsymbol{\varepsilon}}_m - \dot{\boldsymbol{\varepsilon}}_m^v) \right.$$
$$\left. + \mathbb{M}_*^{e^{-1}} \cdot \left\{ \dot{\boldsymbol{\varepsilon}}_m - \mathbb{M}_*^v \cdot (\mathbf{s}_i - \mathbf{s}_m) \right\} \right] \tag{18}$$

where $\mathbf{s}_m$ (resp. $\mathbf{s}_i$) denotes deviatoric part of $\boldsymbol{\sigma}_m$ (resp. $\boldsymbol{\sigma}_i$). From the consistency equation $<\dot{\boldsymbol{\varepsilon}}> = \dot{\bar{\boldsymbol{\varepsilon}}}$, the strain rate in the matrix $\dot{\boldsymbol{\varepsilon}}_m$ is found and henceforth, the strain rate in the inclusion $\dot{\boldsymbol{\varepsilon}}_i$. The macroscopic stress tensor $\bar{\boldsymbol{\sigma}}$ and the corresponding deviator $\bar{\mathbf{s}}$ are defined by volume averaging over all phases:

$$\bar{\boldsymbol{\sigma}} = <\boldsymbol{\sigma}>, \qquad \bar{\mathbf{s}} = <\mathbf{s}>. \tag{19}$$

More details can be found in (Mercier and Molinari, 2009), especially for the presentation of the algorithm to perform update of all variables during the loading process. The respective equiva-

lent formulation of the Mori–Tanaka scheme for the sequential approach can be found in (Kowalczyk-Gajewska and Petryk, 2011).

3. Finite element analysis

Two numerical models of particulate composite microstructure have been constructed in the ABAQUS/STANDARD software. These two models are classically adopted in the literature. The first model is a single inclusion unit cell model following earlier works by Doghri and Ouaar (2003); Chaboche et al. (2005); Pierard and Doghri (2006) or Lahellec and Suquet (2007). This unit cell is also widely adopted for the validation of yield surfaces for porous materials, see for instance (Koplik and Needleman, 1988). The first numerical model will be denoted as FEM-1. In our contribution, inclusions have spherical shape, see Fig. 4 (a). The ratio c of the inclusion volume to the unit cell volume corresponds to the volume content of the inclusion phase in the composite. Since uniaxial tension–compression loadings will be considered next, the problem can be analyzed in two dimensions (axisymmetric approach). A mesh with reduced integration, linear 4-node axisymmetric elements (CAX4R in ABAQUS) is used to discretize the total FEM domain with a refinement near the matrix-inclusion interface. In the case of 25% of inclusion phase content, 1775 (resp. 750) elements are used to mesh the inclusion (resp. matrix) domain.

Since such a unit cell represents a strong simplification of the real microstructure; a 3D representative volume element is also considered in the following. In this case, 30 non-overlapping spherical inclusions are randomly distributed within a cubic domain, see Fig. 4 (b). The second numerical model will be denoted as FEM-30. The volume content of the 30 spheres corresponds to the volume content c of the inclusion phase in the composite. This type of volume element was also analyzed by Pierard et al. (2007) and Lahellec and Suquet (2013). As presented in (Smith and Torquato, 1988), a random sequential additive scheme (RSA) is adopted to define the present RVE with 30 spheres distributed using a pseudo-random number generator. The radius (assumed identical for all spheres) is calculated so as to obtain the prescribed volume fraction of particles. Note that the minimum distance between particle centers is taken as 2.07 times the sphere radius. In our approach, the RVE presents a periodic structure with respect to the three cubic axes. So the part of a sphere that is falling off an edge of the RVE is wrapped around to the opposite edge. As a consequence, the geometries of two opposite faces are identical.

For the 3D RVE, two inclusion volume fractions are considered: 10% and 25%. The unit cell is meshed using standard 10-node full integration tetrahedra (C3D10 in ABAQUS). A mesh sensitivity study has been performed on the case of 25% inclusion volume content with three mesh densities: $65,000$, $150,000$ and $280,000$ total number of elements. Two configurations with different phase contrasts have been tested to asses mesh sensitivity. For a composite with elastic inclusion embedded in an elastic–viscoplastic matrix ($m = 0.1$), results have revealed very little mesh sensitivity. Less than 2% difference on the overall stress has been observed when considering the $150,000$ FE or the $280,000$ FE models. When both phases have elastic–viscoplastic behaviors, no difference was noticeable on the overall response between the coarse and fine meshes. As a consequence, the intermediate mesh density has been adopted to present FEM results with sufficiently good confidence. Thus, the FE model contains approximately 1250 elements per inclusion in the case of 25% inclusion volume content and 500 elements in the case of 10%. Note also that such 3D representation of material microstructure leads to more time consuming computations. For both representations (2D or 3D models) geometric nonlinearities are disregarded since a small deformation formalism has been adopted in the theory. The FE domain extent is $L \times L$ for 2D case and $L \times L \times L$ for the 3D, see Fig. 4.
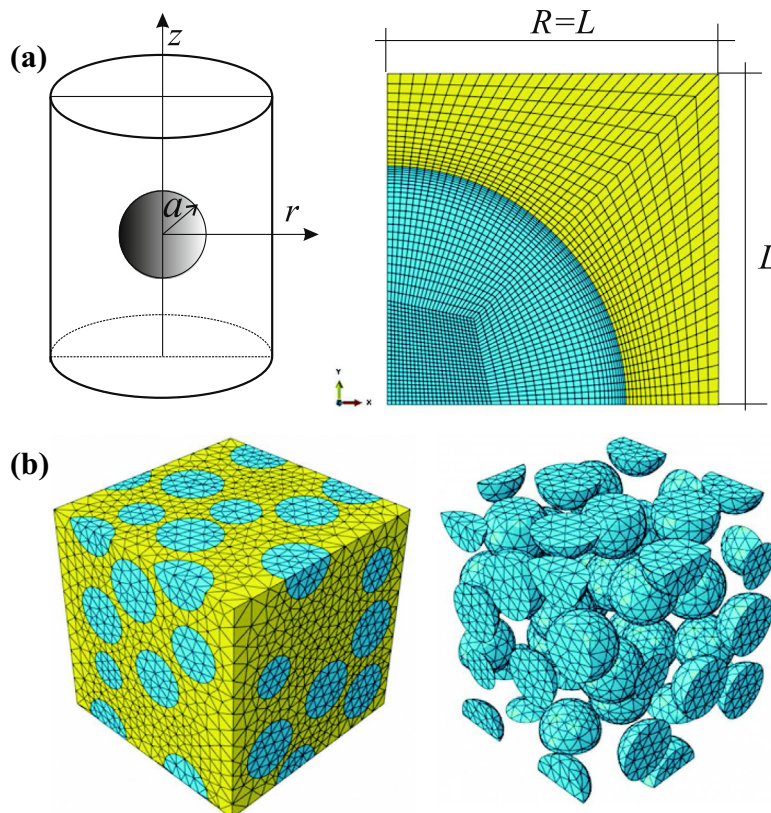

Fig. 4. Presentation of the two numerical models for the composite microstructure. (a) A cylindrical unit cell (FEM-1); (b) a representative volume element with 30 inclusions (FEM-30).

Uniaxial cyclic tension–compression loadings are considered in the paper so the following boundary conditions are prescribed at the remote boundary of the RVEs. For the axisymmetric cell, a constant axial velocity $v_z(r, L, t) = \pm \dot{\varepsilon} L$ is imposed while tangential stresses are set to zero on this face, $\dot{\varepsilon}$ being the nominal strain rate. The lateral surface remains vertical during deformation so the radial displacement of each material point of the surface is identical while a zero overall traction force is applied. To preserve symmetry, no vertical displacement is allowed on the bottom surface. For the 3D case, let us consider for instance that the loading direction is parallel to the unit vector $\mathbf{e}_z$. The upper surface is subjected to constant velocity $v_z(x, y, z = L, t) = \pm \dot{\varepsilon} L$, with zero tangential stress. The displacement of the opposite face is maintained equal to zero in the z direction. Lateral surfaces remain vertical, with zero overall traction force. Note that calculations have also been performed in $\mathbf{e}_x$ and $\mathbf{e}_y$ loading directions.

4. Comparison

4.1. Selection of a RVE

The chosen random set of spheres and the loading direction may have an effect on the overall response of the microstructure. So as to define a reference configuration that may represent the average response of the composite cell, an accuracy analysis similar to the one of (Pierard et al., 2007) has been conducted. Two realizations containing 25% volume fraction of inclusions with different spatial arrangements have been loaded in uniaxial tension at a strain rate $\dot{\varepsilon} = 10^{-2} s^{-1}$ along the three axes of the reference frame. Elastic inclusions embedded in an elastic–viscoplastic matrix (material parameters listed in Table 1 with $m = 0.1$) is considered first. This infers that 6 numerical simulations have been carried out from which the mean response has been computed. The configuration (realization and loading direction) which leads to the closest response when compared to the mean one, has been selected as the reference configuration. Note that the maximum relative difference for the overall stress between all configurations did not exceed 1.5% (the reference configuration exhibits about 0.35% difference to the mean value). With use of two point probability functions the statistical homogeneity and isotropy of the retained realization has been analyzed, see Appendix A. With these preliminary analyzes, it is demonstrated that the size of the RVE and the number of inclusions may be sufficiently representative of homogeneous isotropic composite microstructure. Note that the set of sphere centers of the reference configuration has also been adopted for the low inclusion volume content case $c = 0.1$. The sphere radius has been adjusted to reach the required volume fraction of inclusions.

4.2. Uniaxial tension

Comparisons of results of FE analysis with the predictions obtained using approximate interaction law combined with different micro–macro transition schemes have been performed for uniaxial tension process. The extreme contrast in viscous properties of the phases is assumed, i.e. inclusions are elastic, while the matrix is elastic-viscoplastic. The associated viscoplastic behavior

is described by a power-law (11). Different strain rate sensitivities for the matrix phase and different volume contents of inclusions are tested. Material parameters used in the analysis can be found in Table 1. Results are shown in Fig. 5. The purpose of this analysis is to evaluate the accuracy of the additive tangent Mori–Tanaka scheme in the present context. In all Figs. 5–18, stress and strain values (overall or local) correspond to components aligned with the loading direction.

For $m = 1$, both FE results (FEM-1 and FEM-30) are stiffer than predictions obtained by the additive tangent Mori–Tanaka scheme, see Fig. 5 (a). This result was already mentioned in (Lahellec and Suquet, 2007) where the set of material parameters was identical but a plane strain loading was considered. For this linear viscous case, calculations can be also performed using the exact interaction rule (3) formulated in LT space in conjunction with the Mori–Tanaka method. It enables to separate the effect of an approximate
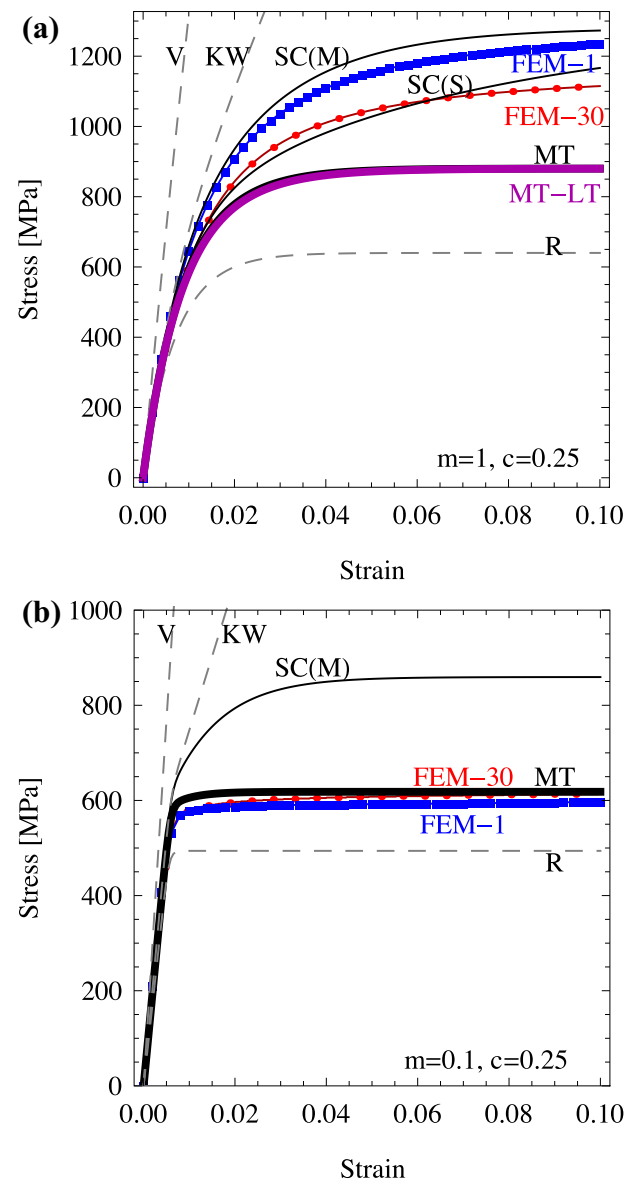

Fig. 5. Macroscopic response in uniaxial tension with a strain rate $\dot{\varepsilon} = 10^{-2}$ s^{-1} for a two-phase composite with 25% of inclusion phase. Material parameters are collected in Table 1: (a) $m = 1$, (b) $m = 0.1$. Notation: R – Reuss, V – Voigt, KW – Kroner-Weng, MT – additive tangent Mori–Tanaka, MT-LT – Mori–Tanaka solved in LT space, SC(M) – self-consistent with the additive interaction rule, SC(S) – self-consistent with the sequential interaction rule with an additional accommodation step, FEM-1 – unit cell, FEM-30 – RVE with 30 inclusions.

Table 1
Material parameters adopted for the composite where the inclusion behavior is elastic and the matrix is elastic–viscoplastic (the flow stress is described by a power law relationship (11)).

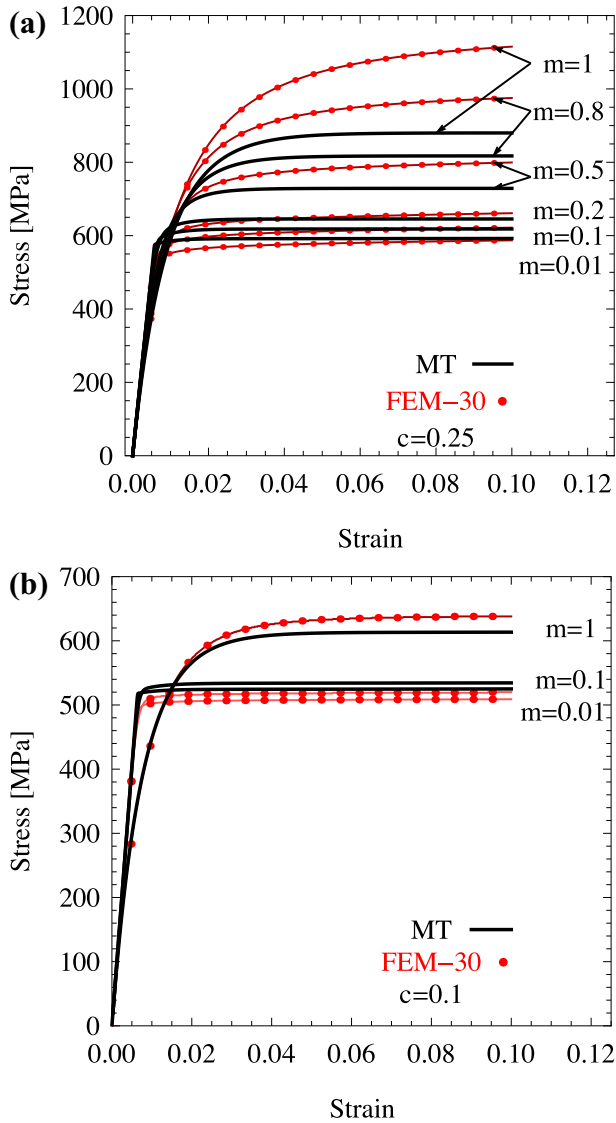| Phase	E [GPa]	v	σ_Y [MPa]	$\dot{\varepsilon}_0$	m
Matrix	70	0.3	480	0.01	1, 0.8, 0.5, 0.2, 0.1, 0.01
Inclusion	400	0.2	–	–	–

Fig. 6. Effect of the strain rate sensitivity of the matrix phase on the macroscopic response. Predictions based on the additive tangent Mori–Tanaka approach are compared to results of the FEM-30 model. A uniaxial tension process at the strain rate $\dot{\varepsilon} = 10^{-2}$ s^{-1} is considered. A two-phase composite with elastic inclusions is tested. Material parameters are collected in Table 1: (a) $c = 25\%$, (b) $c = 10\%$.

Fig. 7. Stress–strain responses for the composite, inclusion and matrix phases in a single tension–compression cycle with a strain amplitude $\varepsilon_a = \pm 0.1$ and a strain rate (a) $\dot{\varepsilon} = 10^{-2}$ s^{-1} and (b) $\dot{\varepsilon} = 10^{-4}$ s^{-1}. Predictions based on the proposed additive tangent Mori–Tanaka approach are compared to results of the FEM-30 model. A two-phase composite with 25% of inclusion phase is adopted. Material parameters are collected in Table 1; $m = 0.1$.

interaction rule from the effect of an averaging scheme. Comparing the curves marked by MT and MT-LT one observes that the difference between the two schemes is negligible. Consequently, the origin of the discrepancy between FE results and homogenization technique is mostly inherited from the averaging scheme. Predictions of the Voigt and Reuss approaches, of the Kroner-Weng and self-consistent models are also reported on Fig. 5 (a). In addition, results for two variants of the self-consistent averaging scheme developed for elastic–viscoplastic materials are shown: the first one corresponds to the additive tangent interaction rule (for a detailed formulation see (Mercier and Molinari, 2009)) and the second one to the sequential model with an additional accommodation step discussed in more detail in (Kowalczyk-Gajewska and Petryk, 2011). A huge difference in prediction is captured by choosing different homogenization techniques. This illustrates the fact that the considered case is really difficult to model due to the large contrast in phase behavior. It has to be noticed that a considerable discrepancy between the two FE models (the axisymmetric unit cell and the RVE with 30 inclusions) is observed as well. The overall response obtained using the RVE with 30 inclusions is
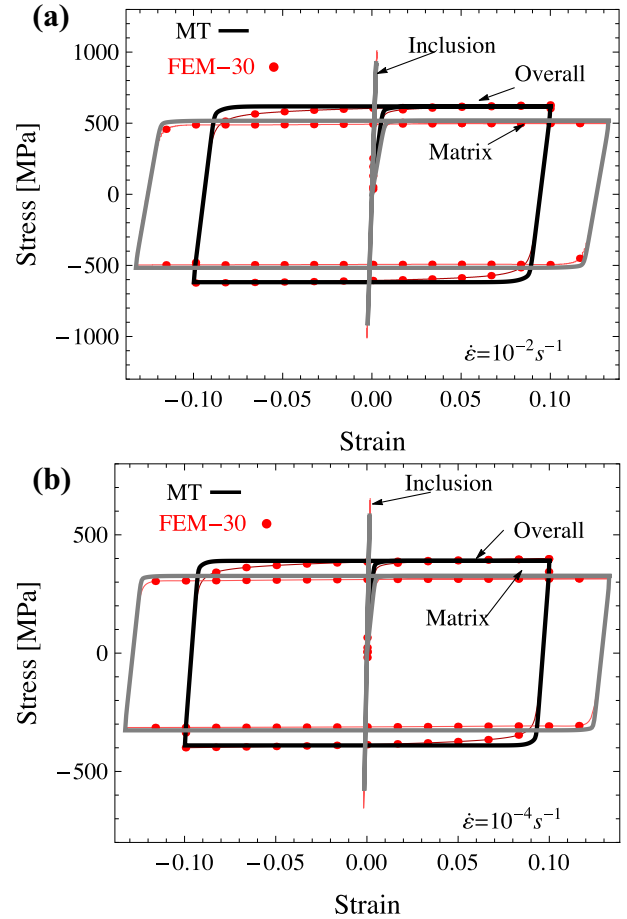
significantly softer than when adopting axisymmetric unit cell. Thus, the question of the selection of a computational RVE for this highly rate-sensitive case can be raised.

For $m = 0.1$, it is observed in Fig. 5 (b) that the proposed additive tangent Mori–Tanaka scheme is able to predict with good accuracy the macroscopic stress strain response given by the FEM-30 model, while other classical averaging schemes like Voigt, Reuss, Kroner–Weng, the tangent self consistent, are clearly not salient for such case. For self-consistent model, this discrepancy is due to the representative volume element selected in FE calculations, which is representative of a composite (inclusion + matrix) microstructure. It is well established that the Mori–Tanaka averaging scheme is more adequate in that case. It has to be mentioned that a secant version of the proposed additive MT interaction law has been also developed. As expected, the macroscopic response is then much stiffer (results not presented in Fig. 5 (b) than the ones obtained by FE method or the additive tangent MT scheme. This result is consistent with the known studies for viscoplastic materials, where it is observed that secant estimate tends to the Taylor model predictions in the rate-independent limit, that is for $m \rightarrow 0$ (e.g. (Molinari et al., 2004) for the inclusion problem or (Bornert et al., 2001) for polycrystals).

Since it is found that for a composite with elastic inclusions, the predictive capacity of the model is strongly varying with the value of the strain rate sensitivity of the matrix phase, a parametric study is performed. From Fig. 6 (a), it is observed that the additive
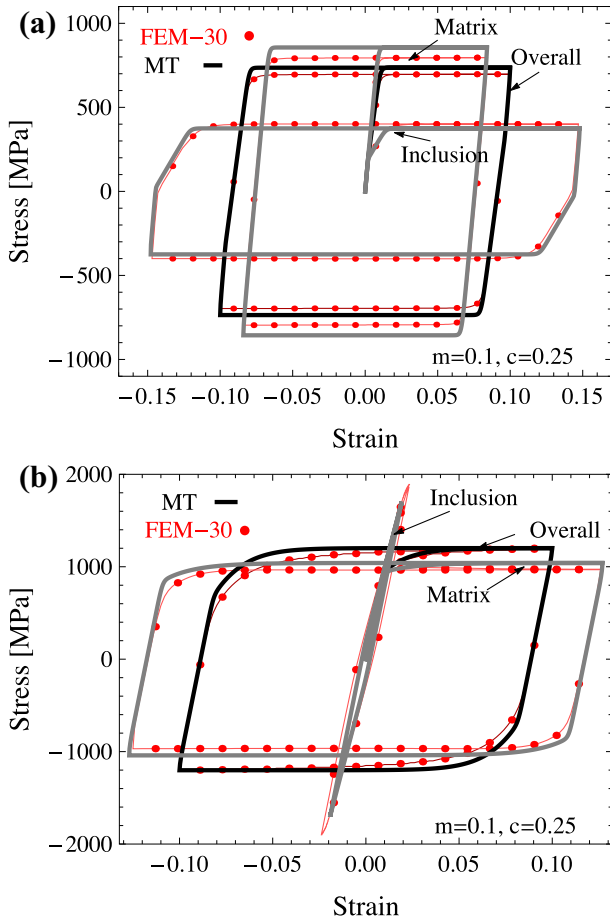
Fig. 8. Stress–strain curves for the composite, inclusion and matrix phases during a single tension–compression cycle with a strain amplitude $\varepsilon_a = \pm 0.1$ and a strain rate $\dot{\varepsilon} = 0.5 \text{ s}^{-1}$. Predictions based on the proposed additive tangent Mori–Tanaka approach are compared to results of the FEM-30 model. A two-phase composite with 25% of inclusion phase is considered. Material parameters are presented in Table 2 ($m = 0.1$) (a) Soft inclusion, (b) Hard inclusion.

tangent Mori–Tanaka scheme provides good predictions of the overall response, as compared to FE analysis, for a low strain rate sensitivity ($m = 0.01, m = 0.1$ and $m = 0.2$), even for moderate volume content of inclusions ($c = 0.25\%$). Discrepancy between predictions increases with larger m values. It does not contradict the established feature that with the proposed approximate additive interaction law and for the linear case ($m = 1$), the analytical solution of the Eshelby problem is recovered. This is exemplified in Fig. 6 (b), where a low volume fraction of inclusions ($c = 10\%$) is tested. In that case, a good approximation of the macroscopic response of the two phase composite is obtained for both low ($m = 0.01$ or 0.1) and large ($m = 1$) values of the strain rate sensitivity.

Our goal is to investigate the efficiency of the additive tangent Mori–Tanaka scheme for metallic material applications (so with low strain rate sensitivity). It seems that the chosen averaging scheme is well suited for our purposes. To validate the proposition, in the next subsections, further validations will be conducted considering cyclic tension–compression loadings. Next, only results obtained with the FEM-30 numerical model will be considered.

4.3. Uniaxial tension–compression cycle

Tension–compression cycle with a constant strain rate up to a specified strain amplitude is analyzed. Material parameters of the previous subsection are adopted, see Table 1. Overall composite

response and stress–strain response per phase are depicted in Fig. 7 for $c = 25\%, m = 0.1$ and two different strain rates: $\dot{\varepsilon} = 10^{-2} \text{ s}^{-1}$ (Fig. 7 and $\dot{\varepsilon} = 10^{-4} \text{ s}^{-1}$ (Fig. 7 (b). It is seen that quality of predictions obtained with use of the additive tangent Mori–Tanaka scheme is similarly accurate for the considered strain rates. In general the overall stress level in the composite and the stress level in the matrix phase are correctly assessed. Noticeable difference is observed only during transient regimes when the loading direction is reversed (change of sign of the strain rate). The maximum average stress level in the inclusion phase is slightly under-predicted as compared to FE analysis.

Next, a new configuration is analyzed. The inclusion and the matrix phases have elastic–viscoplastic behavior. Elastic properties are the same for matrix and inclusions. The power-law relationship (11) is adopted for the description of viscoplasticity. Two different cases are considered: a *hard inclusion* case, i.e. $\sigma_Y^i / \sigma_Y^m = 5$ and a *soft inclusion* case, i.e. $\sigma_Y^i / \sigma_Y^m = 0.2$. Superscript i (resp. m) refers to properties of the inclusion (resp. matrix) phase. All material parameters for this analysis are collected in Table 2. Note that the material description and properties have been proposed by Lahellec and Suquet (2007) but the composite was subjected to a monotonic process under a different loading path (in plane shear strain). For the cyclic loading, the strain amplitude is equal to $\epsilon_a = 0.1$ and the strain rate $\dot{\varepsilon} = 0.5 \text{ s}^{-1}$. In Fig. 8, the macroscopic behavior and the response per phase are presented for a 25% volume content of inclusion. The strain rate sensitivity is set to $m = 0.1$. In the case of *soft inclusion*, the overall stress–strain response is well predicted, see Fig. 8 (a). The local response for the inclusion and the matrix is also precisely predicted. Since the inclusion is soft with $\sigma_Y^i / \sigma_Y^m = 0.2$, the total strain cumulated inside the inclusion is larger than in the matrix phase. On the contrary, the stress level within the inclusion phase is lower. Trends of the finite element calculations are captured with a good accuracy. For the *hard inclusion* case, see Fig. 8 (b), the predictions remain satisfactory. For soft and hard inclusions with the considered set of material parameters, it is seen that the elastic–viscoplastic transition (from elastic response to viscoplastic response) where magnitudes of the elastic and viscous strain rates are comparable, is well captured, especially for the overall response and the matrix phase.

Table 2
Material parameters for the two elastic–viscoplastic phases. Viscoplasticity is described by adopting a power-law relation (11).

Phase	E [GPa]	ν	σ_Y [GPa]	$\dot{\varepsilon}_0$	m
Matrix	100	0.45	1	1	0.1
Inclusion	100	0.45	5/0.2	1	0.1

In the final example of this section, the viscoplastic flow law based on the Perzyna-type model is adopted, see Eq. (16). Material parameters for the two phases are collected in Table 3. Almost similar material properties were adopted by Pierard and Doghri (2006). With this model, the viscoplastic flow begins when the equivalent stress reaches first a threshold value σ_Y. Therefore accurate estimation of the level of stress within the elastic–viscoplastic phases is crucial to determine the plastic strain. Indeed, even small differences in stress level can result in significant differences in strain when the equivalent stress value is close to the threshold. In Fig. 9 (a,b) the overall stress–strain response of a composite with 10% and 25% of inclusions is compared to finite element results.

Table 3
Material parameters for the inclusion and matrix phases. Viscoplasticity is described by the Perzyna-type law (16).

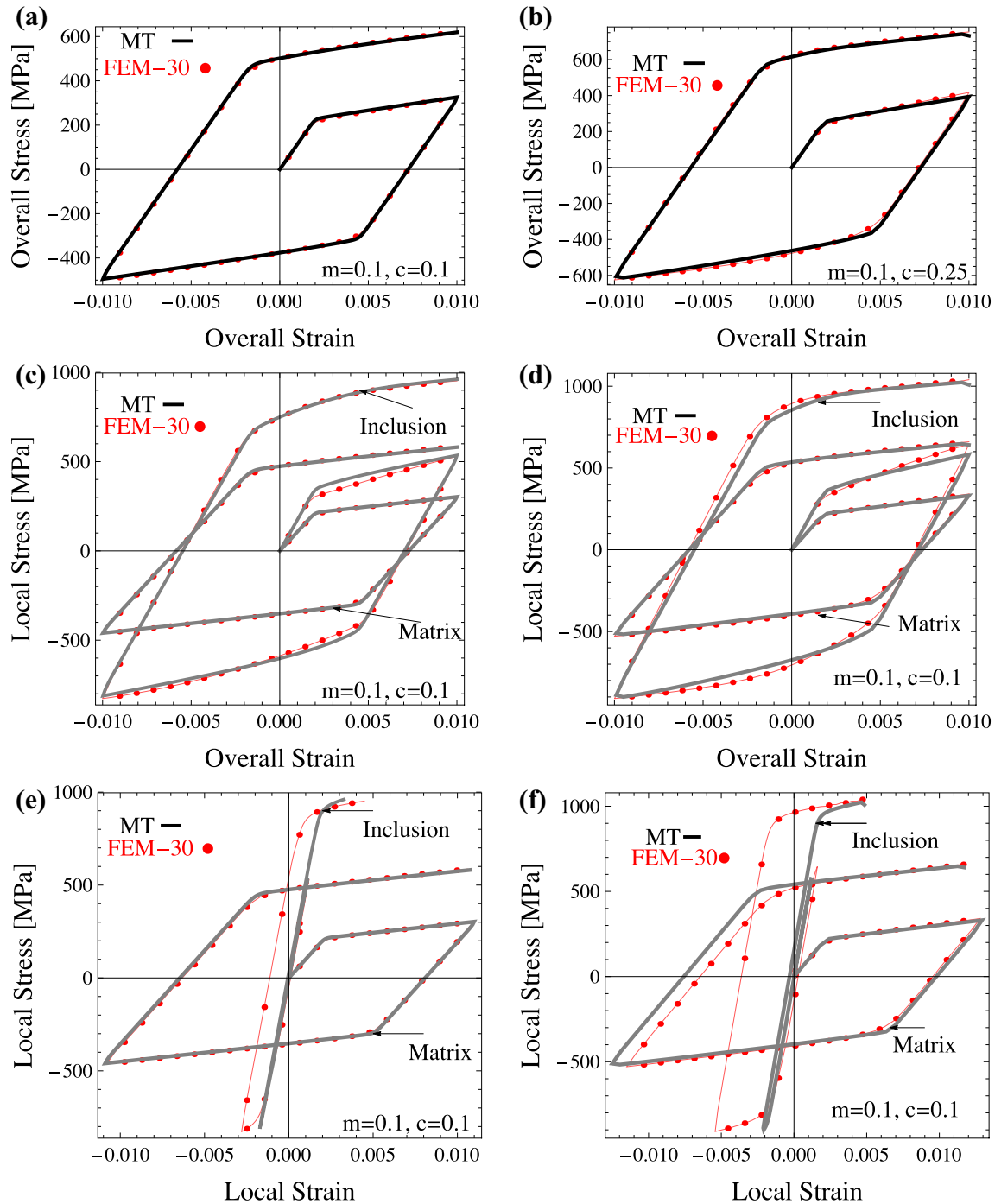| Phase	E [GPa]	ν	σ_Y [MPa]	k [GPa]	n	$\dot{\varepsilon}_0$ [s^{-1}]	m
Matrix	100	0.3	100	5	1	$0.3 \cdot 10^{-3}$	0.1
Inclusion	500	0.3	500	5	1	$0.3 \cdot 10^{-3}$	0.1

Fig. 9. Macroscopic (a,b) and local (c,d,e,f) responses in a single tension–compression cycle with a strain amplitude $\varepsilon_a = \pm 0.01$ and a strain rate $\dot{\varepsilon} = 10^{-3}$ s^{-1}. Predictions based on the proposed additive tangent Mori–Tanaka approach are compared to results of the FEM-30 model. Two-phase composite with 10% (a,c,e) and 25% (b,d,f) of inclusion phase are considered. Material parameters are listed in Table 3 ($m = 0.1$).

A good agreement between approaches is observed, even for the larger volume fraction $c = 25\%$. Fig. 9 (c,d) present the local stress in both phases versus the overall longitudinal strain. In this case, we observed that the stress level in both phases is well predicted by the additive tangent Mori–Tanaka approach, when compared to FE results. It has to be mentioned that this type of representation is usually adopted in the literature. In Figs. 9 (e,f), additional results are presented since local stress–strain responses of both phases are shown. Differences between results of the finite element method and the Mori–Tanaka model are observed. Indeed, as already stated, the stress level is well predicted while the strain magnitude

in both phases is not so precisely captured, especially in the inclusion phase. Note that for the considered case, the difference is only visible when the results are presented in the form of Figs. 9 (e,f) (local stress versus local strain). According to FE analysis, inclusions develop plasticity during the compression part of the cycle, while for the homogenization model, plasticity is initiated only during the second reverse loading (second tension). Note that a tension–compression asymmetry of the stress–strain loop in the inclusion is obtained. It increases when the increasing volume content of inclusions. Macroscopically, it could result in kinematic hardening phenomenon.
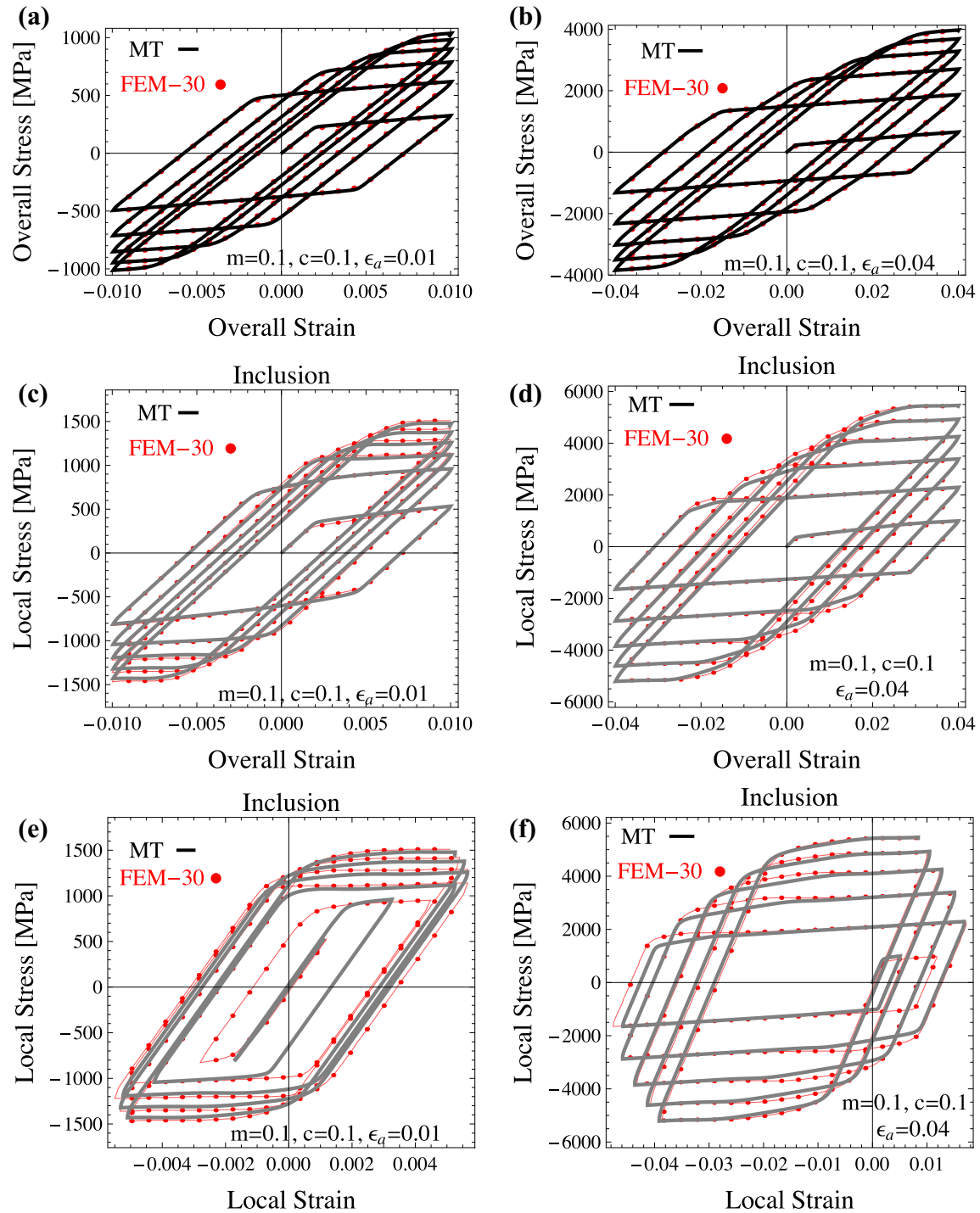
Fig. 10. Stress–strain curves for a two phase composite with 10% of inclusion phase. (a,b) Macroscopic response (c,d) stress in the inclusion phase versus overall strain (e,f) stress–strain in the inclusion domain. Multiple tension–compression cycles with a strain amplitude $\varepsilon_a = \pm 0.01$ (a,c,e) and $\varepsilon_a = \pm 0.04$ (b,d,f) for a strain rate $\dot{\varepsilon} = 10^{-3}$ s^{-1} are adopted. Predictions based on the proposed additive tangent Mori–Tanaka approach are compared to results of the FEM-30 model. Material parameters are listed in Table 3 ($m = 0.1$).

4.4. Multiple tension–compression cycles

In the example presented at the end of the previous subsection, we have observed that in the case of Perzyna-type viscoplasticity, differences between FE and homogenization results can be observed for the stress–strain response in the inclusion phase during the first cycle depending whether the stress threshold level is achieved or not. Indeed, in finite element calculations, plasticity initiates in an heterogeneous manner in the inclusion domain,

while of course, with the Mori–Tanaka approach, only average values can be captured. So clearly, the initiation of plasticity, is difficult to capture when compared to steady state viscous regime. Therefore, it is necessary to check if the difference in strain predictions observed during the first cycle propagates during cyclic loading. The effect of the magnitude of the strain amplitude is also investigated. When the strain amplitude is small enough, then the first unloading can take place during the transient regime when elastic and viscous strain increments are of comparable
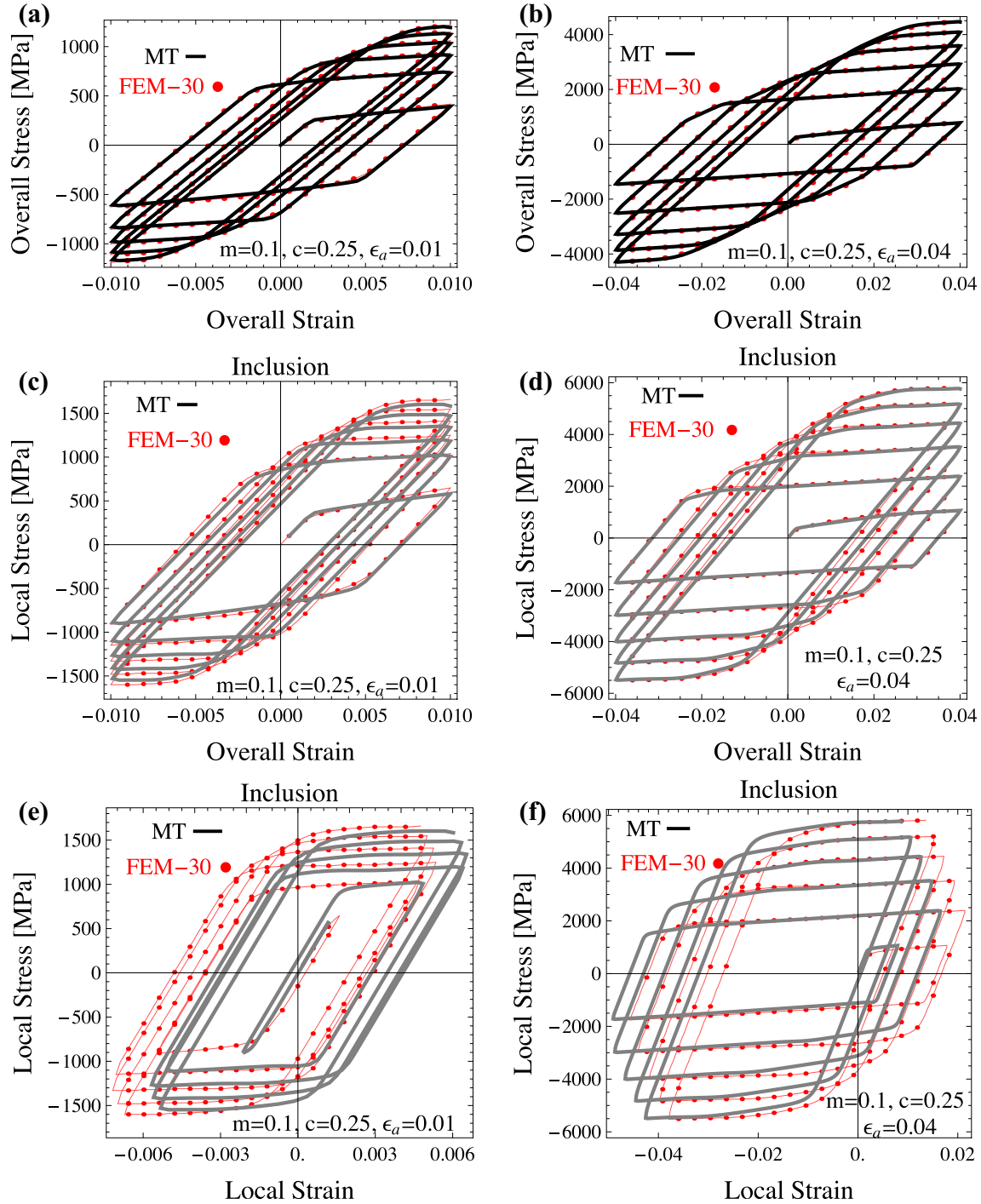
Fig. 11. Stress–strain curves for a two phase composite with 25% of inclusion phase. (a,b) Macroscopic response (c,d) stress in the inclusion phase versus overall strain (e,f) stress–strain in the inclusion domain. Multiple tension–compression cycles with a strain amplitude $\varepsilon_a = \pm 0.01$ (a,c,e) and $\varepsilon_a = \pm 0.04$ (b,d,f) for a strain rate $\dot{\varepsilon} = 10^{-3}$ s^{-1} are adopted. Predictions based on the proposed additive tangent Mori–Tanaka approach are compared to results of the FEM-30 model. Material parameters are listed in Table 3 ($m = 0.1$).

magnitude (Fig. 1). In this regime, it is clear that significant differences between the homogenization scheme and FE results may occur.

Fig. 10 (a,b) presents the overall response for five tension–compression cycles with two different strain amplitudes: $\varepsilon_a = 0.01$ and $\varepsilon_a = 0.04$. The volume content of inclusions is small, i.e. 10%. Excellent agreement between the two approaches is obtained as concerns the overall composite response. Differences are observed at the level of individual phases, see Fig. 10 (e,f) for the local stress – local strain loops in the inclusion phase. It is found that, although

for the first cycle significant discrepancy is obtained in the prediction of the plastic strain development in the inclusion phase (see differences between Figs. 10 (c,d) on the one hand and Figs. 10 (e,f) on the other hand), the accuracy of the Mori–Tanaka predictions as compared to the FE analysis increases with subsequent cycles. A better agreement between the two analyzes is achieved when the strain amplitude is larger, so when the first reverse loading occurs at a stage of well-developed viscous flow. Similar results for $c = 25\%$ and for two strain amplitudes $\varepsilon_a = 0.01$ and
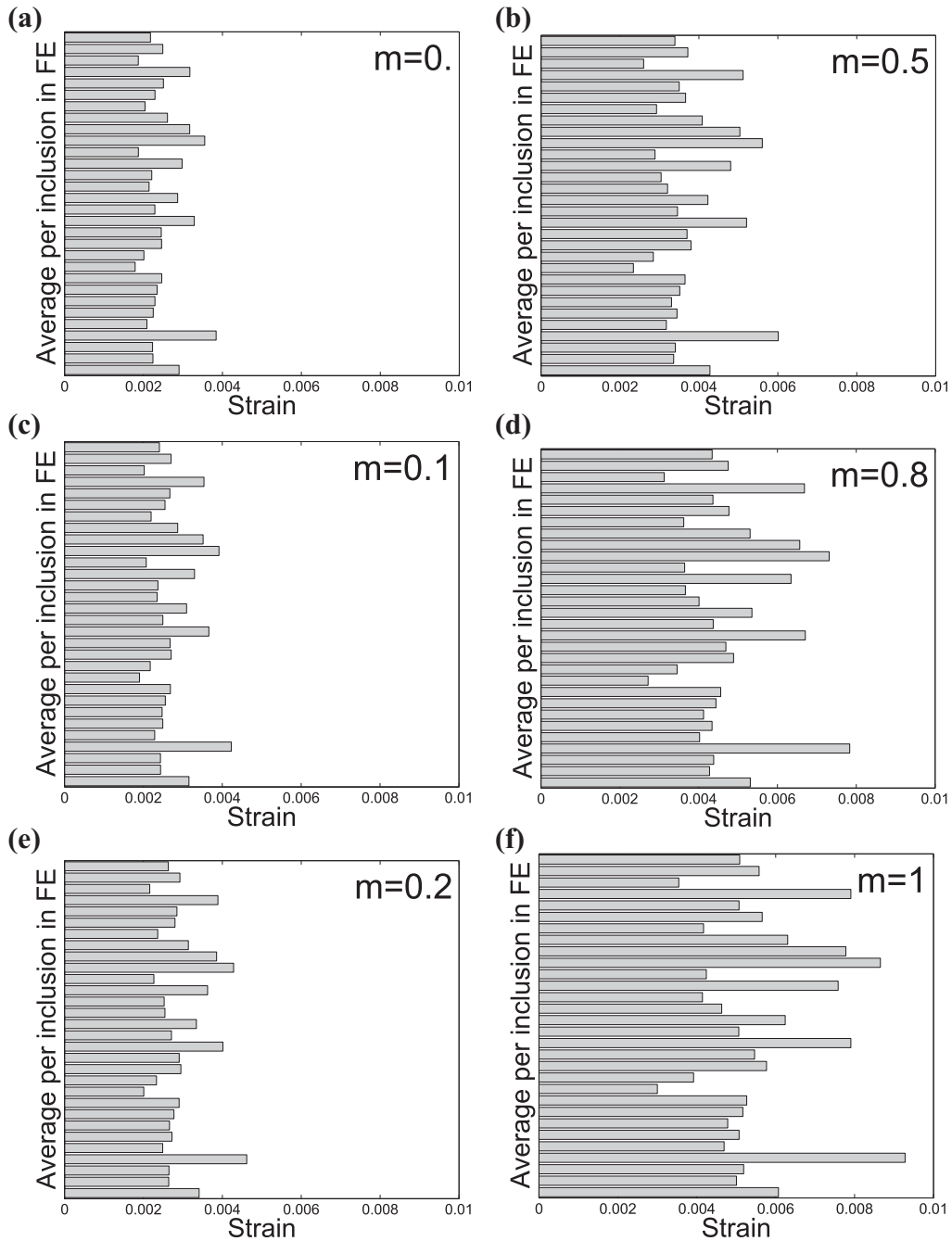
Fig. 12. Influence of the matrix strain rate sensitivity m on the strain heterogeneity in all individual inclusions in FE analysis. Average values per inclusion are calculated at the end of the tensile loading of Fig. 6 where the macroscopic uniaxial strain is $\varepsilon_a = 0.1$. The inclusion is elastic and the matrix is elastic–viscoplastic following a power-law strain rate dependency. Calculations are carried out for a two-phase composite with 25% of inclusions. Material parameters are collected in Table 1. The macroscopic strain rate is $\dot{\varepsilon} = 0.01s^{-1}$.

$\varepsilon_a = 0.04$ are shown in Fig. 11. Although the volume content of inclusions is increased, the agreement in the overall response is still excellent. The stress level in the inclusion phase is also well estimated by the MT method as compared to the FE predictions. Similarly to previous cases, the largest discrepancy is observed in estimating strains in the inclusion phase. For $c = 0.25$, stress–strain cycles for the inclusion phase derived by the two approaches (MT versus FE) appear to be similar in shape; a translation along the strain axis is necessary to superimpose both curves. So clearly, the centers of the cycles are not identical. The difference in strain prediction is mostly inherited from the first few cycles.

To study cyclic response in more detail, we define the strain amplitude in the inclusion $\Delta\varepsilon_i^k$ during cycle k, as the difference

between the longitudinal strain in the inclusion at the end of the tensile part of cycle k (for the overall strain ε_a) and the corresponding strain at the end of the compressive part of cycle k (when the overall strain is $-\varepsilon_a$). We also define the stress amplitude in the inclusion $\Delta\sigma_i^k$ as its counterpart for the longitudinal stress. Note that only information concerning the inclusion phase is provided since the discrepancy is mostly observed for the inclusion domain. For a volume fraction of $c = 0.1$ and the two overall strain amplitudes $\varepsilon_a = 0.01$ and 0.04 (cases of Fig. 10), it is observed in Table 4 that $\Delta\varepsilon_i^k$ and $\Delta\sigma_i^k$ computed from FEM-30 model are satisfactory retrieved after few cycles. Table 4 clearly enlightens that a difference exists during the first cycle (see for instance $\Delta\varepsilon_i^1$ with $\varepsilon_a = 0.01$) and decreases with additional cycles. When $\varepsilon_a = 0.04$
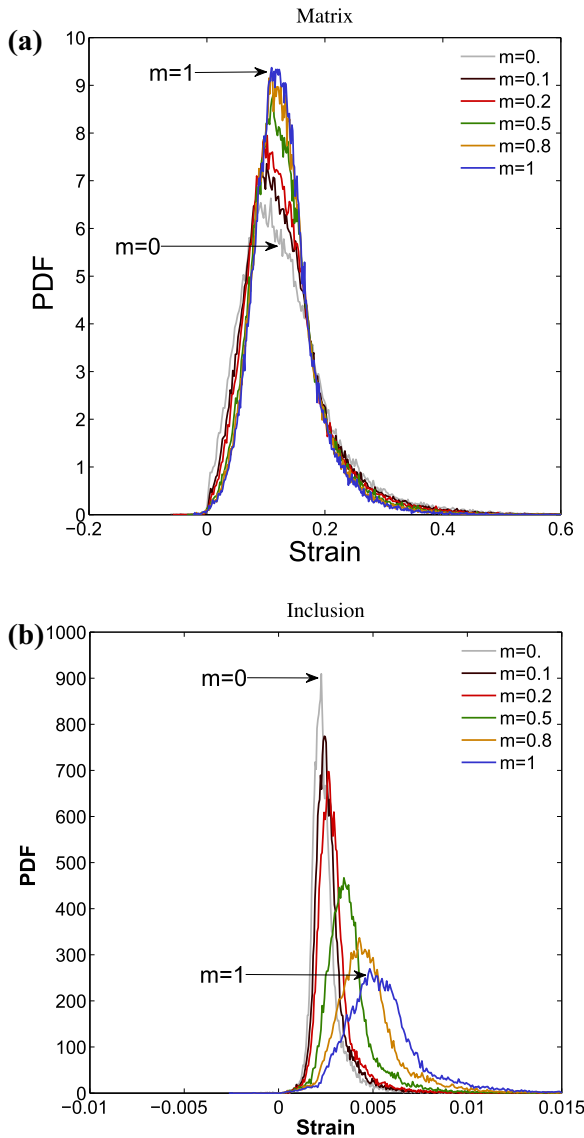
Fig. 13. Probability density functions (PDF) presenting the local strain in the (a) matrix phase and (b) inclusion domain in FE analysis for different values of the strain rate exponent m. The inclusion is elastic and the matrix is elastic–viscoplastic following a power-law strain rate dependency. Calculations are made for a two-phase composite with 25% of inclusions and material parameters collected in Table 1. Uniaxial tension up to a macroscopic strain of $\varepsilon_a = 0.1$ at macroscopic strain rate $\dot{\varepsilon} = 0.01 s^{-1}$ is performed as in Fig. 6.

even for the first cycle, predictions are accurate. For the configuration of Fig. 11 where the volume fraction of inclusions is $c = 0.25$, some discrepancies are observed for the strain amplitude. When $\varepsilon_a = 0.04$, less than 10% difference is observed after five cycles. When $\varepsilon_a = 0.01$, difference is reducing with cycles. The stress amplitude $\Delta \sigma_i^k$ is accurately predicted even for the first cycle. The reasonable predictions of the strain and stress amplitudes in the inclusion is an important result and should have some interest when adopting the additive tangent Mori–Tanaka approach for fatigue problems.

5. Heterogeneity aspects

The proposed homogenization method can predict only average strains and stresses whereas a strong heterogeneity in the mechanical fields may develop at the level of the individual constituents. FE analysis allows the knowledge of the heterogeneous strain or stress fields in the whole domain. In this section, numerical results have been analyzed to describe heterogeneity at different scales. First, the average strain and stress per phase (volume average over the inclusion or matrix domains) are provided. In addition to this overall response, we propose to quantify the heterogeneity between inclusions. So a first level of heterogeneity is obtained by considering the mean value in each individual inclusion, see Eq. (B.1) for its definition. A second level of heterogeneity is portrayed by a probability density function summarizing how heterogeneity is developed in the whole inclusion domain, see Appendix C. This two stages of heterogeneity enable to have a clear view of stress and strain fluctuations within the inclusion domain. It has to be mentioned that such results are not often presented in research works dealing with the validation of a homogenization scheme. One of exceptions is Moulinec and Suquet (2003) who studied the effect of the hardening exponent on the intraphase heterogeneity of the strain field in a two phase composite cylinder assemblage (2D representation). The two phases were incompressible with an elastic–plastic behavior (power-law model without rate dependency and the same hardening exponent). The inclusion material was harder than the matrix phase. The loading applied to the 2D unit cell was a shear stress. The authors underlined that the inclusion phase was relatively homogeneously strained whatever the hardening exponent value. They also drew the attention upon the tendency to strain localization for highly non linear materials (low hardening exponent value).

In the present paper, the heterogeneity of strain and stress response of the two configurations of Sections 4.2 and 4.4 is analyzed in the following.

Table 4
Strain and stress amplitudes ($\Delta \varepsilon_i^k$, $\Delta \sigma_i^k$) in the inclusion phase for subsequent cycles k predicted by the Mori–Tanaka method and by the FEM-30 model.

|	Mori–Tanaka/ FEM-30				
cycle k	1	2	3	4	5
$c = 0.1, \epsilon_a = 0.01$					
$\Delta \epsilon_i^k [\times 10^{-2}]$	0.28/0.39	0.75/0.83	1.05/1.08	1.10/1.10	1.06/1.06
$\Delta \sigma_i^k$ [MPa]	1345/1357	2004/2002	2312/2360	2582/2650	2810/2890
$c = 0.1, \epsilon_a = 0.04$					
$\Delta \epsilon_i^k [\times 10^{-2}]$	5.09/5.27	6.27/6.27	5.87/5.83	5.40/5.34	4.96/4.91
$\Delta \sigma_i^k$ [MPa]	2646/2639	5172/5100	7250/7160	8876/8800	10144/10100
$c = 0.25, \epsilon_a = 0.01$					
$\Delta \epsilon_i^k [\times 10^{-2}]$	0.33/1.33	0.99/2.35	1.21/2.19	1.21/1.96	1.27/1.73
$\Delta \sigma_i^k$ [MPa]	1483/1557	2136/2190	2478/2580	2779/2890	3036/3150
$c = 0.25, \epsilon_a = 0.04$					
$\Delta \epsilon_i^k [\times 10^{-2}]$	5.70/5.35	6.52/6.06	6.14/5.66	5.71/5.23	5.31/4.85
$\Delta \sigma_i^k$ [MPa]	2795/2830	5373/5370	7533/7530	9273/9300	10671/10720
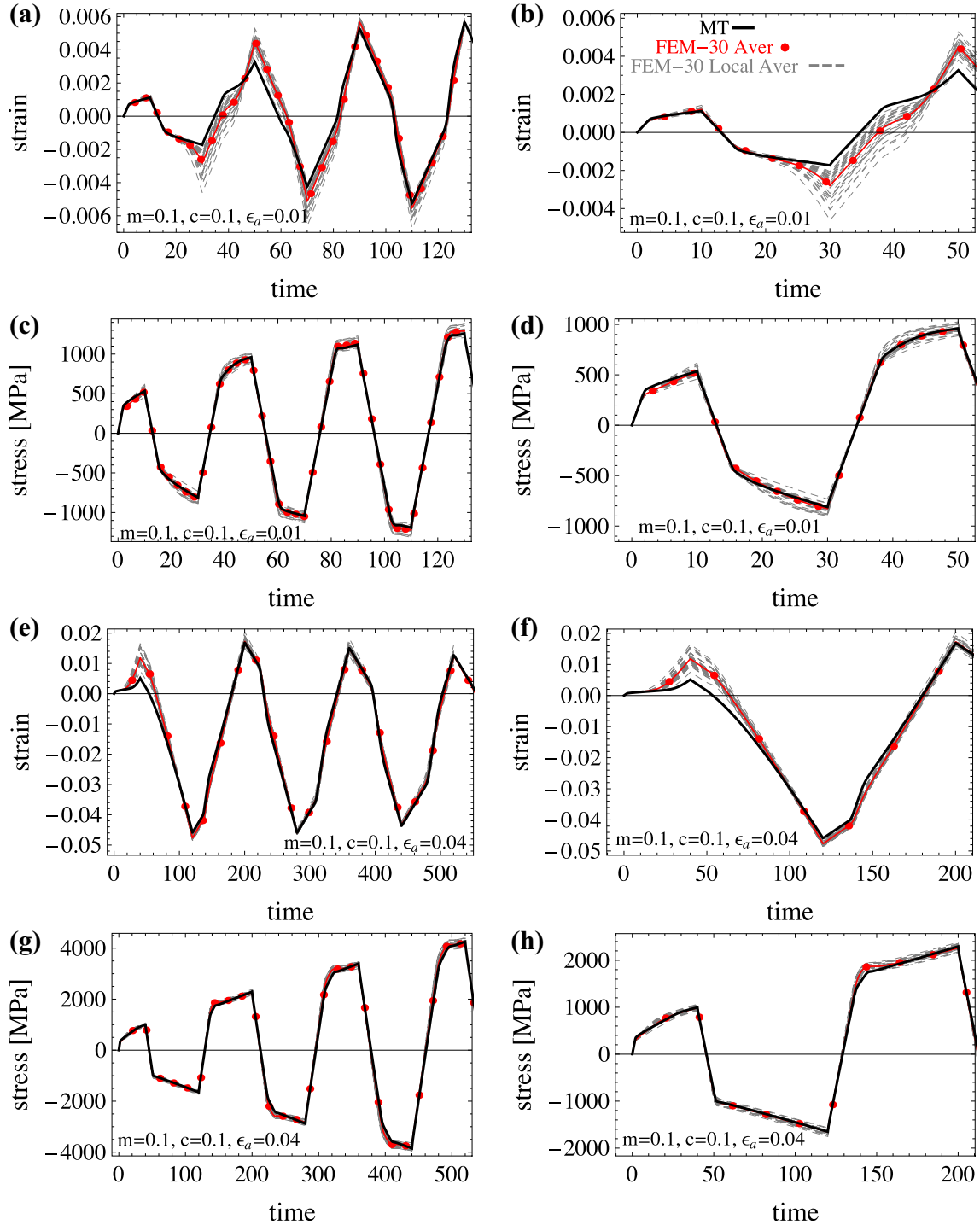
Fig. 14. Time evolution of the heterogeneity of strains (a,b,e,f) and stresses (c,d,g,h) among all individual inclusions in finite element calculation for a two-phase composite with 10% of inclusions. Overall responses provided by the additive tangent Mori–Tanaka scheme and obtained by FEM-30 are also presented. The legend in the subfigure (b) applies to all subfigures. Material parameters are collected in Table 3 ($m = 0.1$). The composite is subjected to cyclic loading of Fig. 10. In Figs. (a–d), the strain amplitude is $\varepsilon_a = 0.01$. For Figs. (e–h), the strain amplitude is larger: $\varepsilon_a = 0.04$.

5.1. Elastic inclusion in an elastic viscoplastic matrix

The selected case refers to the high contrast configuration of Section 4.2 where the inclusion phase is elastic and the matrix material is elastic-viscoplastic, see Fig. 6. Parameters are given in Table 1. The composite material is subjected to a uniaxial tension at $\dot{\varepsilon} = 10^{-2}s^{-1}$ up to an overall strain of $\varepsilon_a = 0.1$. The volume fraction of inclusions is 25%. In the present work, the effect of the strain rate parameter m on the fluctuation in strain and stress

fields in each phase is studied. As shown in a previous section, discrepancy between MT and FEM-30 in the overall response may be highly marked, especially when the matrix phase has a large value of m. The development of heterogeneities that is not captured by the homogenization scheme may explain the relative discrepancy observed in Figs. 5 and 6.

So as to quantify heterogeneities between particles, the average strain in each of the 30 inclusions is first shown in Fig. 12. One observes that for highly sensitive matrix material ($m = 0.8$ or 1),
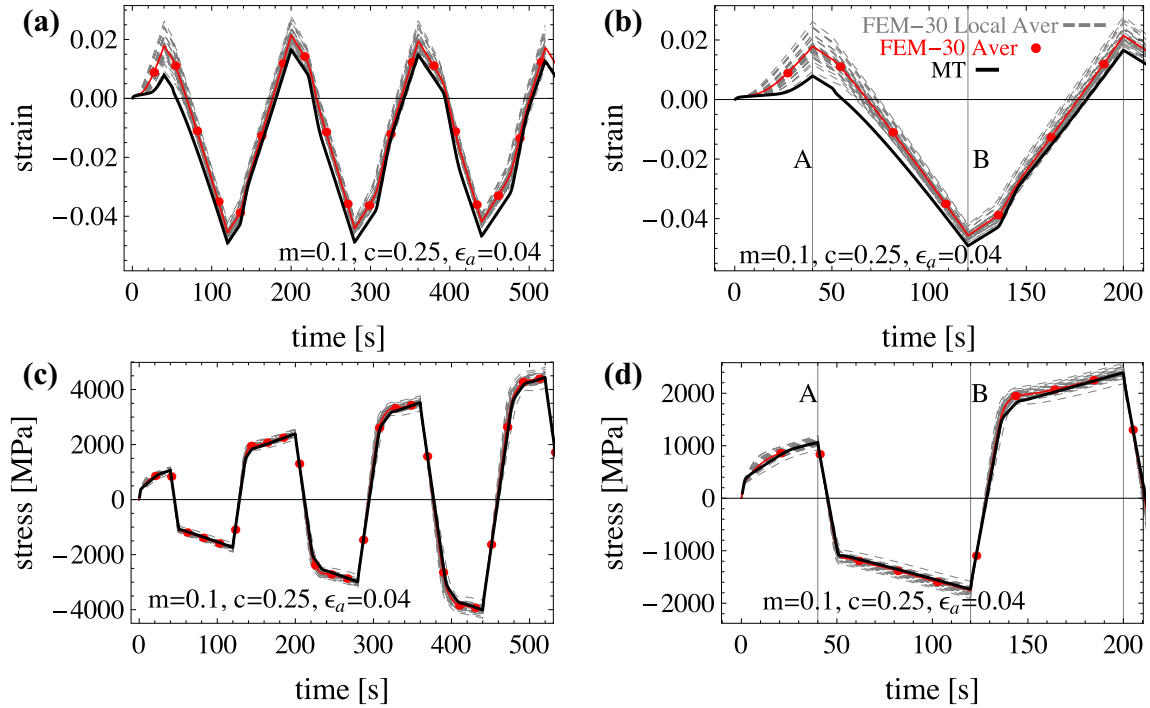
Fig. 15. Time evolution of the heterogeneity of strains (a,b) and stresses (c,d) among all individual inclusions given by finite element calculation for a two-phase composite with 25% of inclusions. Overall responses provided by the additive tangent Mori–Tanaka scheme and obtained by FEM-30 are also presented. The legend in the subfigure (b) applies to all subfigures. The composite is subjected to cyclic loading of Fig. 11. Material parameters are collected in Table 3 ($m = 0.1$). The strain amplitude is $\varepsilon_a = 0.04$.

the heterogeneity is more pronounced. When $m = 1$, it is observed that the average strain calculated in the most deformed inclusion is three times larger than the one in the least deformed inclusion. When $m = 0$, the ratio decreases to a value of two. Note that for $m = 0$, the matrix phase is elastic-perfectly plastic with a yield stress equal to 480 MPa.

Probability density functions characterizing uniaxial strain heterogeneity are given in Fig. 13 for the two phases. For the matrix domain, it is observed that whatever the m value, probability density functions are quite similar, Fig. 13 (b). Indeed, the phase contrast (elastic-viscoplasticity for the matrix and elasticity for the inclusion) leads to the development of a limited strain magnitude in the inclusion phase, such that the matrix mean strain is close to the imposed overall strain weighted by its volume fraction. For the studied case, the mean uniaxial strain in the matrix obtained from FEM-30 is about 0.1306, a value close to $\varepsilon_a/(1-c) = 0.1333$.

In the inclusion domain, an increase of the matrix rate sensitivity m leads to a larger strain heterogeneity (see Fig. 13 (a). It is also shown that the distribution of uniaxial strain is broader for $m = 1$ and sharper for $m = 0$. As a consequence, moderate accuracy of the additive tangent Mori–Tanaka scheme is observed when m is large (i.e. when the strain heterogeneity in the inclusion is large). The present conclusion is only valid when the inclusion is elastic and the matrix is elastic viscoplastic.

5.2. Elastic viscoplastic matrix and inclusion

The configuration of Fig. 10 is adopted where the two phases have an elastic–viscoplastic behavior. The viscoplasticity is described by the Perzyna law, see Eq. (16). The rate sensitivity is set to $m = 0.1$. The composite material is subjected to cyclic loading with a strain amplitude of $\varepsilon_a = \pm 0.01$ or $\varepsilon_a = \pm 0.04$. The volume fraction of inclusions is 10%.

Fig. 14 provides time evolutions of the average uniaxial strain in each of the 30 inclusions and of the strain value derived by the proposed additive Mori–Tanaka scheme. We discuss first the case where the strain amplitude during cycles is equal to $\varepsilon_a = 0.01$, see Figs. 14 (a–d). During the first tensile loading, inclusions remain mostly elastic (as also observed in Fig. 10 (e). As a consequence, the strain value in all inclusions is quite homogeneous close to the value given by the proposed additive Mori–Tanaka scheme. Differences start to develop during the first unloading. For the Mori–Tanaka approach, the inclusion domain remains elastic. From FEM-30 model, one observes that the heterogeneity in stress–strain response leads to a complex situation where only part of the inclusion domain develops plasticity. Therefore, for any mean field averaging scheme it will be difficult to precisely describe this situation. After 30 s of loading, when the total strain is −0.01, a large difference in the inclusion strain field is depicted. Due to the low strain rate sensitivity value, the predictions in terms of stresses are more accurate, see Fig. 14 (c,d). During the second cycle (for $t > 90$ s), the strain heterogeneity among individual inclusions decreases and the prediction of the proposed additive MT scheme is more precise. The present analysis explains why after two cycles, only a tiny difference is visible in Fig. 10 (e) in the stress–strain curve for the inclusion domain.

In a second example, the strain amplitude is increased to $\varepsilon_a = 0.04$, other parameters remain unchanged. The whole inclusion domain plastifies after the first loading but still the additive tangent Mori–Tanaka model leads to an underestimate of the strain magnitude in the inclusion domain when $t < 40$ s. However, after the first compression phase ($t \approx 120$ s and $\varepsilon = -0.04$), the strain estimate provided by the Mori–Tanaka scheme is really satisfactory. The strain heterogeneity which exists between inclusions (only during the first cycle) explains results presented in Fig. 10 (f). As already mentioned in the previous section, for low volume fraction of inclusions, when the strain amplitude of the cycle is large enough so that all inclusions plastify during the first loading step, the prediction of
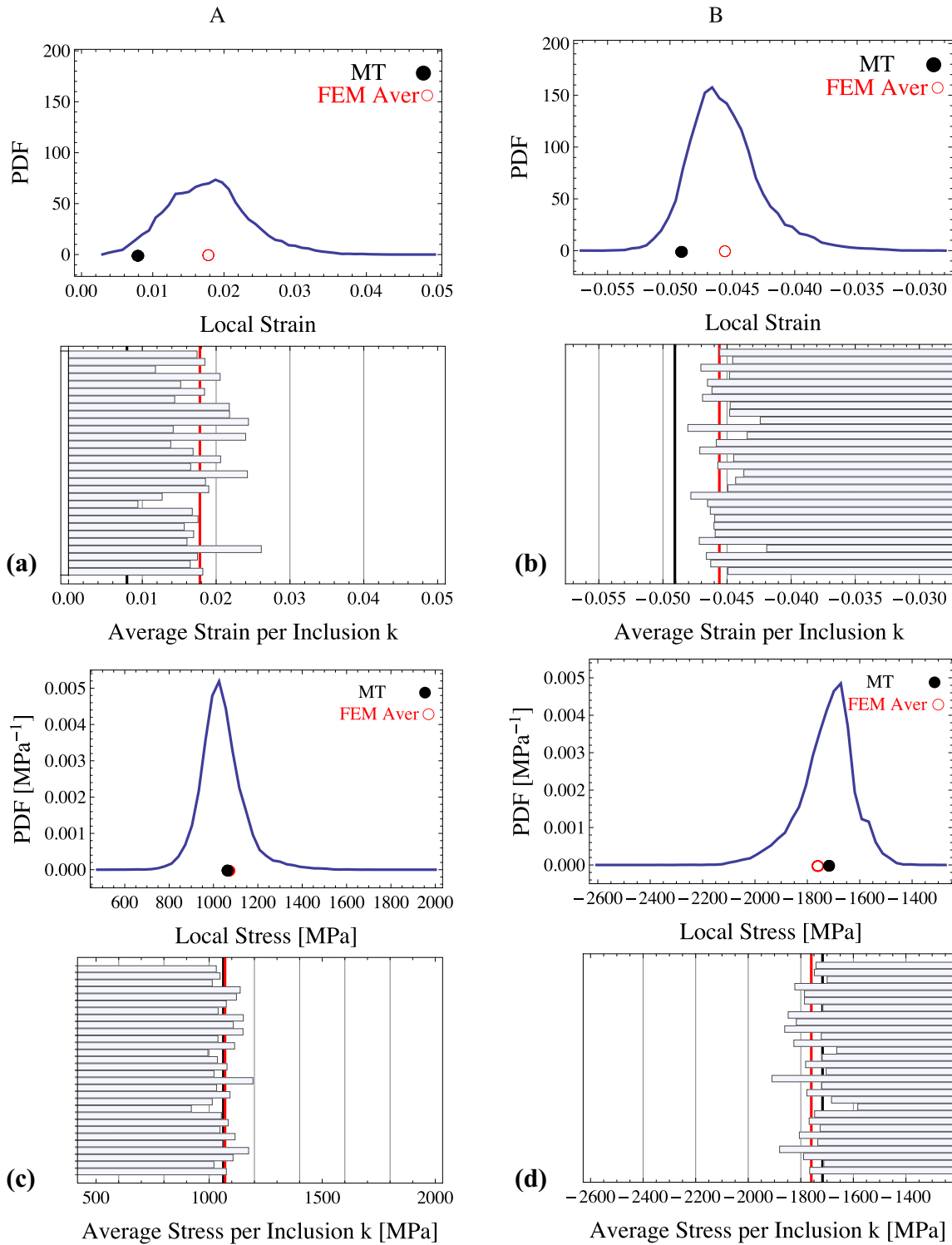
Fig. 16. Probability density function (PDF) presenting the local strain (a,b) and stress (c,d) heterogeneity derived from the FEM-30 model within the inclusion phase, for the two selected times of Fig. 15: (a,c) A ($t = 40$ s) – end of the first tension and (b,d) B ($t = 120$ s) – end of the first compression. Average stress and strain given by the additive tangent MT scheme and by FEM-30 are also presented. A two-phase composite with 25% of inclusions is considered and material parameters are collected in Table 3. The strain amplitude of the cycle is $\varepsilon_a = 0.04$.

the MT scheme is acceptable after the first cycle. On the contrary, when the reverse loading occurs in the regime where elastic and plastic strains in the inclusion are of the same magnitude, then the predictions are less accurate. Nevertheless, after few cycles, prediction will be quite good. Some cycles are necessary to accommodate the deformation and to reduce the heterogeneity.

Next, a larger volume fraction of inclusions ($c = 0.25$) is considered. The strain amplitude is $\varepsilon_a = 0.04$. In this case, it is seen in Fig. 15 that the strain heterogeneity between inclusions is large as compared to the previous case where the inclusion volume fraction has been set to 0.1. It is also observed that the average strain in inclusions during tensile loading (when the macroscopic strain is
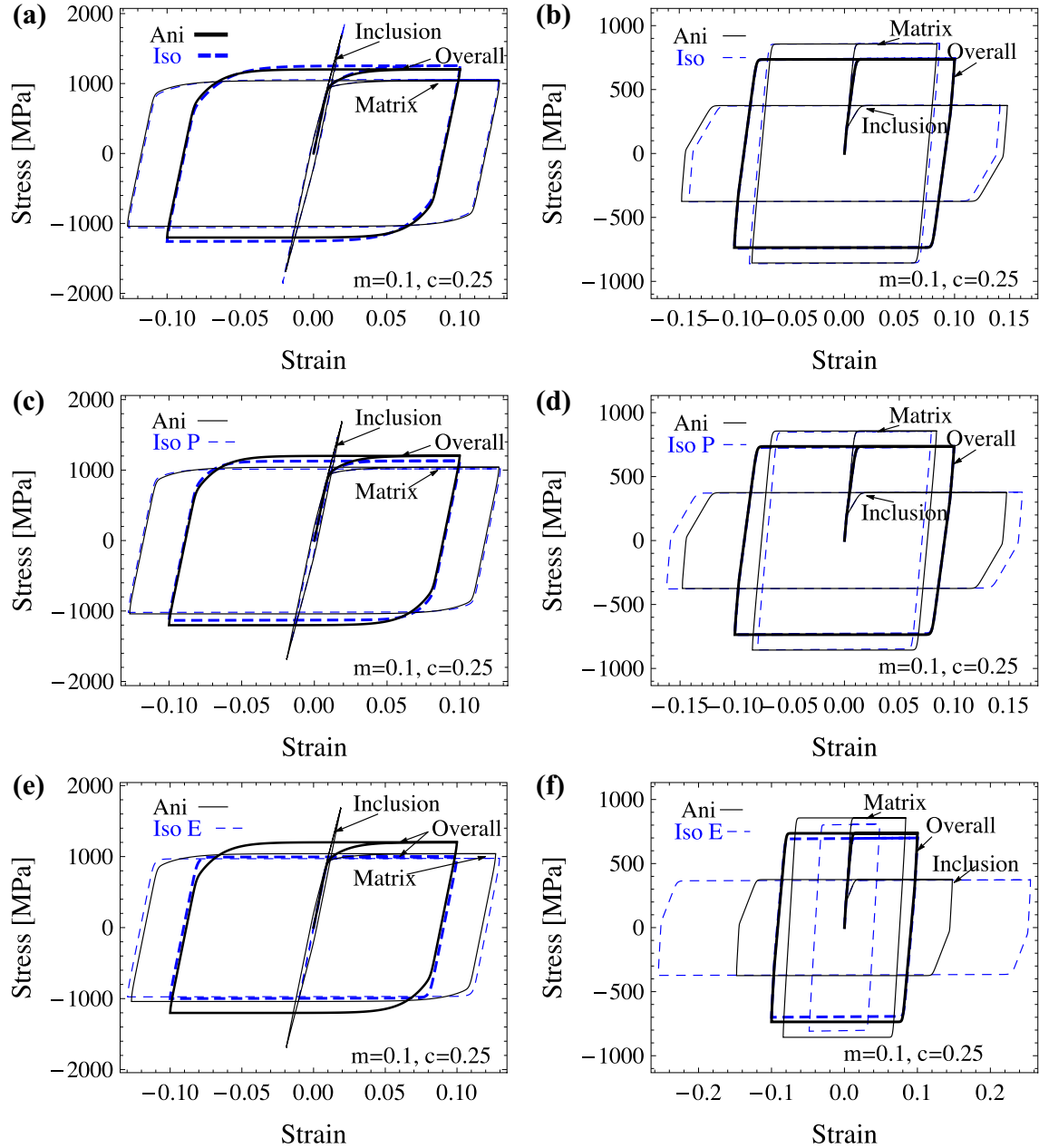
Fig. 17. Macroscopic and local stress strain curves for a single tension–compression cycle with a strain amplitude $\varepsilon_a = \pm 0.1$ and a strain rate $\dot{\varepsilon} = 0.5$ s^{-1}. Predictions based on the proposed additive Mori–Tanaka approach without (Ani) and with isotropization of the Hill tensor (Iso) – (a), of the polarization tensor (Iso P) – (b) and of the Eshelby tensor (Iso E) – (c). A two-phase composite with 25% of inclusion phase is considered. Material parameters are presented in Table 2 ($m = 0.1$). Figures on the left (resp. right) present predictions for the hard (resp. soft) inclusion case.

$\varepsilon = 0.04$), given by FEM-30 model (red curve) is larger than the one predicted by the additive tangent Mori–Tanaka scheme. On the contrary, when the macroscopic strain is $\varepsilon = -0.04$, the strain level in the inclusion domain given by the MT scheme is larger (in absolute value) than the one provided by the FEM-30 model. The results shown in Fig. 15 explain the stress strain responses presented in Fig. 11.

In order to quantify in more detail the strain heterogeneity, the local fluctuation in the inclusion domain is presented in Fig. 16 at $t = 40$ s (when $\varepsilon = 0.04$, represented with a line named A in Fig. 15 (b) and at $t = 120$ s (when $\varepsilon = -0.04$, line B). Fig. 16 (a) shows the probability density function of strain which gives information about the variation of the uniaxial strain inside the inclusion phase. The average strain in each inclusion, the average value of the

corresponding strain in the whole inclusion phase obtained by the MT approach and by the FEM-30 model are also presented. The calculated probability density function is quite broad at time A, meaning that a large heterogeneity in strain is present. In addition, the mean strain predicted by FEM-30 is twice larger than the value predicted by the MT approach. At the end of the first compression step (point B), the difference between FEM-30 and MT schemes still exists but does not exceed 20%. The strain heterogeneity between inclusions is reduced leading to better predictions of the analytical MT approach. The present figure shows, at a given time, the map of heterogeneity which leads to results of Figs. 11 and 15. Owing to the low strain rate sensitivity ($m = 0.1$), the stress heterogeneity is less pronounced, as observed in Fig. 16 (c) (point A) and Fig. 16 (d) (point B). When the volume fraction of inclusions is large (here
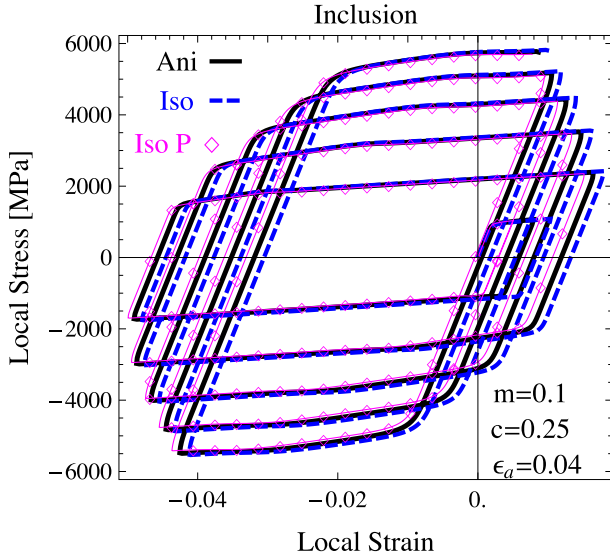
Inclusion

Fig. 18. Comparison of the inclusion response in multiple tension–compression cycles analyzed in Fig. 11 (f) obtained by the Mori–Tanaka approach without (Ani) and with isotropization of the Hill tensor (Iso) or of the polarization tensor (Iso P).

25%), the prediction of the MT scheme is less accurate because of the heterogeneity which exists inside the RVE. The situation is clearly explained within this paper by quantifying the deformation fluctuation inside the inclusion domain. Nevertheless, even for 25% volume fraction of inclusions, as presented in Fig. 11, the overall and average mechanical fields per phase given by the additive tangent Mori–Tanaka scheme provide still reasonable estimates.

6. Effect of isotropization

When materials have elastic–plastic behavior, the *elastic–plastic* tangent operator is anisotropic and predictions of the overall responses are observed to be too stiff. Several authors (Bornert, 2001; Doghri and Ouaar, 2003; Chaboche et al., 2005) have observed that when the Hill or Eshelby or polarization tensors are evaluated by adopting an isotropic approximation of the tangent stiffness, predictions of homogenization technique provide more accurate results. Different strategies of isotropic approximations are available in the literature. The isotropic tangent stiffness is used to evaluate the Eshelby tensor in (Doghri and Ouaar, 2003), while it is used for the polarization tensor in (Chaboche et al., 2005). In this section, the effect of isotropic estimates for the *viscoplastic* tangent stiffness on the quality of predictions is discussed. Since we consider volume preserving viscoplasticity, calculations below are performed in the five dimensional subspace of deviators.

In our paper, owing to a J_2 flow theory, the viscoplastic tangent stiffness $\mathbb{L}^v$ of the matrix is anisotropic for both the power-law or Perzyna law:

$$\mathbb{L}^v = \alpha\mathbb{K} + \frac{3}{2}B\mathbb{G}_s = \left(\alpha + \frac{3}{2}B\right)\mathbb{G}_s + \alpha\mathbb{F}_s \qquad (20)$$

with

$$\alpha = \frac{2}{3}\frac{\sigma^{eq}}{\dot{\varepsilon}^{eq}}, \qquad B = \frac{4}{9}\left(m\frac{\sigma^{eq} - \sigma^{over}}{\dot{\varepsilon}^{eq}} - \frac{\sigma^{eq}}{\dot{\varepsilon}^{eq}}\right). \qquad (21)$$

For the Perzyna law (resp. the power-law), $\sigma^{over} = \sigma_Y + R(\varepsilon^{eq})$ (resp. $\sigma^{over} = 0$). $\mathbb{K}, \mathbb{G}_s$ and $\mathbb{F}_s$ are fourth rank tensors defined as:

$$\mathbb{J} = \frac{1}{3}(\mathbf{1} \otimes \mathbf{1}), \quad \mathbb{K} = \mathbb{I} - \mathbb{J}, \quad \mathbb{G}_s = \frac{2}{3}\left(\frac{\dot{\boldsymbol{\varepsilon}}^v}{\dot{\varepsilon}^{eq}} \otimes \frac{\dot{\boldsymbol{\varepsilon}}^v}{\dot{\varepsilon}^{eq}}\right), \quad \mathbb{F}_s = \mathbb{K} - \mathbb{G}_s, \qquad (22)$$

where $\mathbb{I}$ is a fourth order identity tensor ($\mathbb{K}$ is a corresponding identity tensor for deviatoric second order tensors $\mathbf{s}$, i.e.: $\mathbb{K} \cdot \mathbf{s} = \mathbf{s}$). By analogy to the Zener parameter one can measure anisotropy degree of the viscoplastic tangent stiffness by defining the following factor

$$\xi_s = \frac{\alpha + \frac{3}{2}B}{\alpha} = m\bar{\xi}, \qquad (23)$$

where $\bar{\xi} = 1$ for the power law and $\bar{\xi} = 1/(1 + (\dot{\varepsilon}_{eq}/\dot{\varepsilon}_0)^{-m})$ for the Perzyna-type law. For $m \leqslant 1$, the anisotropy factor ξ_s does not exceed one. The material is isotropic for $\xi_s = 1$. So the anisotropy degree increases with larger non-linearity. The effect of isotropization should be more pronounced for small m-value. An additional increase of the anisotropy degree is observed in the case of the Perzyna-type law with a decreasing $\dot{\varepsilon}_{eq}/\dot{\varepsilon}_0$ ratio.

Different definitions are proposed in the literature for the isotropic tangent stiffness, see for instance (Chaboche et al., 2005). Its definition is not unique. In our paper, $\mathbb{L}^v_{iso}$ is derived from the projection operator proposed for instance in (Bornert, 2001) (i.e. as an isotropic part of a tensor resulting from its harmonic decomposition, see (Forte and Vianello, 1996; Kowalczyk-Gajewska, 2012)). Since we consider volume preserving viscoplasticity, $\mathbb{L}^v_{iso}$ will be simply proportional to $\mathbb{K}$:

$$\mathbb{L}^v_{iso} = 2\mu\mathbb{K} = \frac{1}{5}(\mathbb{K} :: \mathbb{L}^v)\mathbb{K}, \qquad (24)$$

where $\mathbb{K} :: \mathbb{L}^v = K_{ijkl}L^v_{ijkl} = L^v_{ijij} - 1/3L^v_{iijj} = L^v_{ijij}$ is a scalar. Other possibilities were also tested, including the Chaboche et al. (2005) proposal for which $2\mu = \mathbb{G}_s :: \mathbb{L}^v$. None of them resulted in improved predictions as compared to the fully anisotropic case, while the strategy defined in Eq. (24) provided estimates close to the FE predictions.

Combining relationships (20) and (24), $\mathbb{L}^v_{iso}$ is obtained:

$$\mathbb{L}^v_{iso} = 2\mu\mathbb{K} = \left(\alpha + \frac{3}{10}B\right)\mathbb{K}. \qquad (25)$$

In the present paper, the composite material is a two phase material with spherical inclusions. Therefore, with an isotropic tangent stiffness and an incompressible matrix, the Eshelby tensor $\mathbb{E}^v_{iso}$ is simply: $\mathbb{E}^v_{iso} = \frac{2}{5}\mathbb{K}$ and the polarization tensor $\mathbb{P}^v_{iso}$ is $\mathbb{P}^v_{iso} = \frac{1}{5\mu}\mathbb{K}$. Three possibilities of isotropic estimate for the inverse Hill tensor are proposed in the following. First, we consider, as in (Doghri and Ouaar, 2003), that the Eshelby tensor is based on the isotropic tangent stiffness, but all other calculations are performed with anisotropic tensors. As a consequence, a first estimate of the inverse for the Hill tensor $\mathbb{M}^1_*$ is obtained:

$$\mathbb{M}^1_* = \frac{2}{3\alpha}\mathbb{K} - \frac{B}{\alpha\left(\frac{3B}{2} + \alpha\right)}\mathbb{G}_s. \qquad (26)$$

In the second approach, as in Chaboche et al. (2005), the polarization tensor is calculated with the isotropic tangent stiffness (24). A second estimate for the inverse of the Hill tensor $\mathbb{M}^2_*$ is proposed:

$$\mathbb{M}^2_* = -\frac{1}{\alpha - 5\mu}\mathbb{K} + \frac{3B}{2(\alpha - 5\mu)\left(\frac{3B}{2} + \alpha - 5\mu\right)}\mathbb{G}_s. \qquad (27)$$

In the present paper, we also propose to define an inverse isotropic Hill tensor $\mathbb{M}^3_*$ as:

$$\mathbb{M}^3_* = -\left(\mathbb{L}^v_{iso} - (\mathbb{P}^v_{iso})^{-1}\right)^{-1}. \qquad (28)$$

In that case, $\mathbb{M}_*^3$ has a simple form:

$$\mathbb{M}_*^3 = \frac{1}{3\mu}\mathbb{K}. \tag{29}$$

The effect of isotropization has been tested for all cases presented in the paper. Since trends are quite general, we will focused only on the configurations of Fig. 8 and 11.

In the configuration of Fig. 8, the inclusion and the matrix phases have elastic–viscoplastic behavior. The volume fraction of inclusion is $c = 0.25$ and the strain rate sensitivity is $m = 0.1$. Material parameters are summarized in Table 2. For hard inclusion, Fig. 17 shows that the strategy based on the isotropic Hill tensor provides stiffer response than the reference one (with anisotropic tangent stiffness). On the contrary, the response based on the isotropic polarization tensor $\mathbb{P}_{iso}^v$ or on the isotropic Eshelby tensor $\mathbb{E}_{iso}^v$ leads to softer overall response. It could be also noticed that only the approximation with isotropic Eshelby tensor leads to noticeable difference when compared to the reference one (and also to FEM-30, see Fig. 8). Such stiff or soft responses can be understood by noticing that the strain cumulated in the hard inclusion at the end of the first tensile loading (when the overall strain is 0.1), is larger with the isotropic Hill tensor scheme. For the two other schemes with $\mathbb{P}_{iso}^v$ or $\mathbb{E}_{iso}^v$, the strain is reduced; a significant reduction of the stress level is observed in the latter case. For soft inclusion, similar trends concerning the accuracy are observed, but since the inclusion is soft, differences are magnified. Indeed, with the isotropic Eshelby tensor scheme, the strain cumulated in the inclusion is far larger than for the reference one and is not realistic. With the isotropic Hill tensor (resp. polarization tensor) approach, the strain in the inclusion is smaller (resp. larger) than for the reference case. Of course, the situation is reversed for the matrix phase, so as to satisfy prescribed overall strain.

From the present examples (hard or soft), it appears that the reference scheme with anisotropic viscoplastic tangent stiffness provides better agreement with respect to FEM-30 calculations. Results shown in Fig. 17 are for elastic–viscoplastic materials with no strain hardening.

Next, the composite is made of two phases, whose behaviors are described by the Perzyna model (16). Strain hardening is accounted for. The yield stress of the inclusion is larger than the matrix one. The volume fraction of inclusions is $c = 0.25$ and the strain rate sensitivity is $m = 0.1$. Material parameters are listed in Table 3. Cyclic loading of Fig. 11 is considered with a strain amplitude of 0.04. Fig. 18 presents the evolution of strain and stress in the inclusion domain for three versions of the proposed additive tangent Mori–Tanaka scheme: the reference one with anisotropic tangent stiffness, the version with isotropic polarization tensor and the last one with isotropic Hill tensor. Note that results based on the isotropic Eshelby tensor are not presented since predictions are not satisfactory. Owing to the difference in the yield stress of the two phases, the situation is quite similar to the hard inclusion case of Fig. 17. After the first cycle, the strain cumulated in the inclusion by adopting the isotropic Hill tensor is larger than the reference case so it provides better agreement when compared to FEM-30 calculations. But after the reverse loading, the stress–strain curve seems to be better predicted by the full anisotropic approach. After few cycles, both predictions provide similar results, with a shift along the strain axis inherited from the first cycle.

With the present calculations, we have shown that for elastic viscoplastic materials, when the Mori–Tanaka scheme is based on the additive interaction law, isotropization does not improve the quality of predictions. In the literature, the prediction of the tangent self-consistent scheme benefits from the use of anisotropic tangent stiffness, as it is proposed for instance in the VPSC software

(Molinari et al., 1987; Lebensohn and Tomé, 1993). In this section, we have discussed this issue for the proposed additive tangent Mori–Tanaka scheme and the conclusions are similar. Nevertheless, some strategies based on the isotropic Hill tensor or on the polarization tensor can also lead to satisfactory predictions, at least for the considered cases. Therefore, for spherical inclusions, it might be interesting to adopt such isotropization since the Hill tensor can be then specified by an analytical formula. This can be strongly beneficial from a numerical point of view and will help the implementation of such homogenization technique in finite element software.

7. Conclusions

In the present paper, we focus on the predictions of stresses and strains existing in the composite material during various loadings. We consider a two phase material being representative of metal matrix composite. The two phases have elastic–viscoplastic behavior. The mechanical response of the composite is predicted by the Mori–Tanaka scheme combined with the tangent linearization of viscoplastic response and an additive/sequential interaction law proposed by Mercier and Molinari (2009) (see also Kowalczyk-Gajewska and Petryk, 2011). Note that the homogenization theory has been proposed in a general frame so that complex microstructure with a large number of phases can be modeled as well.

Finite element calculations are carried out on a representative volume element containing 30 inclusions. The size of the representative volume element, selected in our approach, is consistent with previous works of the literature, see for instance Pierard et al. (2007). Configurations with a volume fraction of inclusions up to 25% have been tested.

Cyclic loadings in tension/compression with two strain amplitudes are considered. The overall responses given by the additive tangent MT approach and by FEM are compared and are shown to be consistent. The accuracy is increased when the strain rate sensitivity adopts a low value, a condition satisfied when considering metallic materials. As observed by several authors, the case of elastic inclusions embedded in a viscoelastic matrix (with $m = 1$) is complex to model. Some additional developments are still necessary and will be considered in a future work.

The Mori–Tanaka scheme based on the additive interaction law with isotropization of the viscoplastic component has also been considered in the present study. Different strategies of isotropization are adopted and none of them lead to improvement of the accuracy of results when compared to the reference solution (without isotropization).

For most of the cases tested in the present paper, it is shown that the average stress–strain response in each phase can be estimated precisely. Depending on the strain amplitude of the cyclic loading, discrepancy may exist during the first few cycles but after some additional cycles, predictions are observed to be satisfactory, at least for the cases considered in the present paper. Based on the presented results, one can conclude that the additive tangent MT approach is able to predict stress and strain evolutions inside phases satisfactorily. Therefore, the proposed model could be coupled with FE software to give local information on mechanical fields that develop during deformation of structures or during metal forming operation.
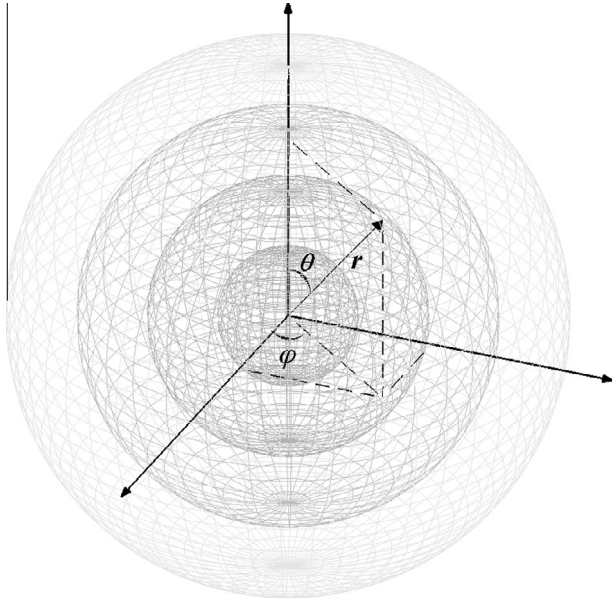
Fig. A.19. Sampling template presenting all investigated directions to evaluate $S_2(\mathbf{r})$. The polar angle is varying from 0 to π and the azimuthal angle from 0 to 2π with increments of $\pi/36$.

Appendix A. Two-point probability function in the RVE

Two-point probability function as a representation of the statistical homogeneity and isotropy of the adopted RVE is presented. The two-point probability function $S_2^{u,v}(\mathbf{x_1}, \mathbf{x_2})$ (Smith and Torquato, 1988; Torquato, 2002) is a measure of the probability to find $\mathbf{x_1}$ lying in phase (u) and $\mathbf{x_2}$ lying in phase (v). For statistically homogeneous media, $S_2^{u,v}(\mathbf{x_1}, \mathbf{x_2}) = S_2^{u,v}(\mathbf{r})$ where $\mathbf{r} = \mathbf{x_2} - \mathbf{x_1}$. For the inclusion matrix composite, where $\{(u), (v)\} = \{(I), (M)\}$, the two-point probability function results in four quantities, namely $S_2^{I,I}(\mathbf{r}), S_2^{M,M}(\mathbf{r}), S_2^{I,M}(\mathbf{r}), S_2^{M,I}(\mathbf{r})$. For statistically homogeneous medium, $S_2^{u,v}$ has the following asymptotic values as $|\mathbf{r}| \to 0$ or $|\mathbf{r}| \to \infty$:

$$
\begin{aligned}
&\lim_{|\mathbf{r}|\to 0} S_2^{I,I}(\mathbf{r}) = c, \\
&\lim_{|\mathbf{r}|\to 0} S_2^{M,M}(\mathbf{r}) = 1 - c, \\
&\lim_{|\mathbf{r}|\to 0} S_2^{I,M}(\mathbf{r}) = \lim_{|\mathbf{r}|\to 0} S_2^{M,I}(\mathbf{r}) = 0, \\
&\lim_{|\mathbf{r}|\to\infty} S_2^{I,I}(\mathbf{r}) = c^2, \\
&\lim_{|\mathbf{r}|\to\infty} S_2^{M,M}(\mathbf{r}) = (1 - c)^2, \\
&\lim_{|\mathbf{r}|\to\infty} S_2^{I,M}(\mathbf{r}) = \lim_{|\mathbf{r}|\to\infty} S_2^{M,I}(\mathbf{r}) = c(1 - c),
\end{aligned}
\tag{A.1}
$$

where c is the inclusion volume fraction and $(1 - c)$ stands for the matrix volume fraction. The proposed analysis aims first at checking whether the actual size of the RVE is suitable to consider the unit
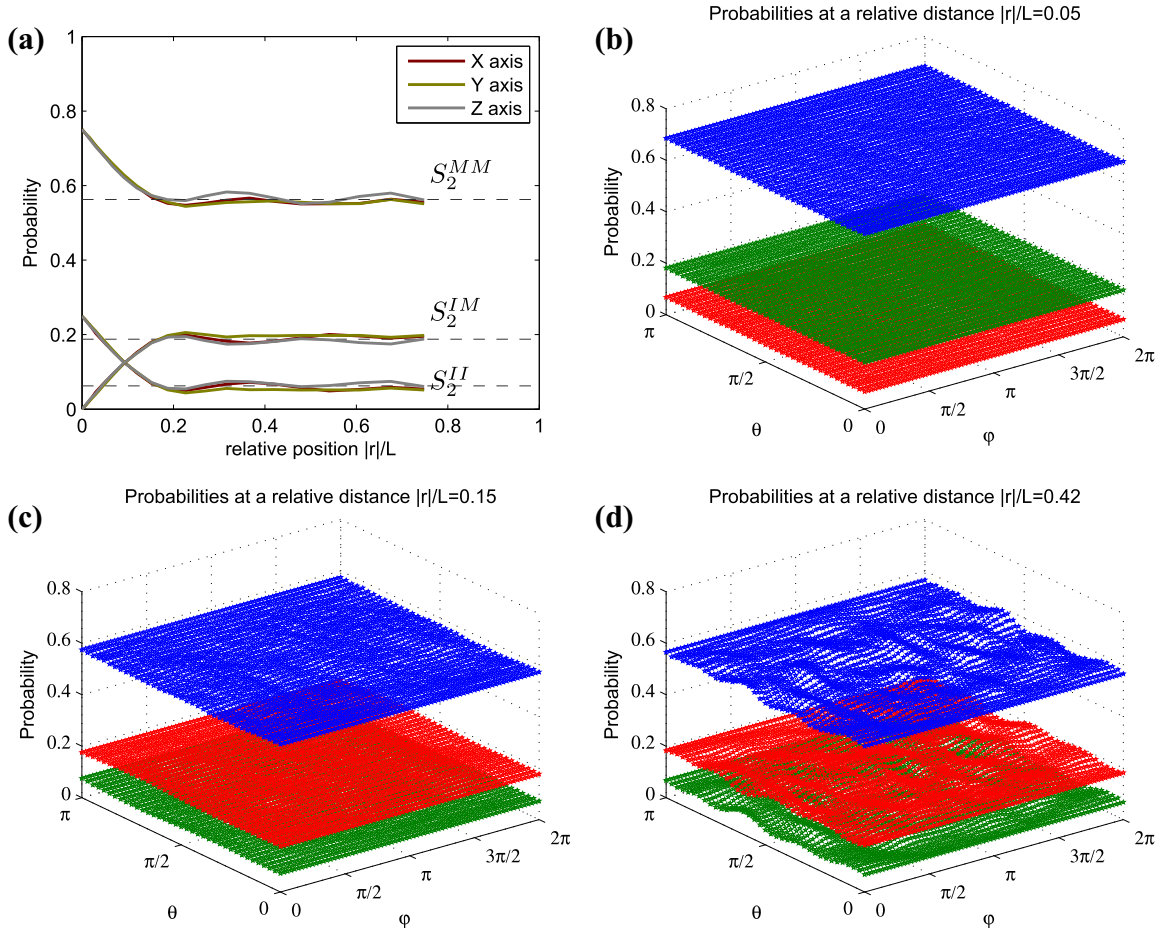

Fig. A.20. Evolution of the two-point distribution functions along the three main axis of the unit cell (a) and maps of $S_2^{I,I}(\mathbf{r}), S_2^{M,M}(\mathbf{r})$ and $S_2^{I,M}(\mathbf{r})$ for different values of $|\mathbf{r}|/L$ (b-d). Results illustrate the statistically homogeneity and isotropy of the RVE made of 30 inclusions.

cell as statistically homogeneous, *i.e.* whether conditions (A.1) are satisfied.

The statistical isotropy of the unit cell is also analyzed. To this end, $S_2^{u,v}(\mathbf{r})$ is evaluated for different directions (identified by the polar and azimuthal angles) by tossing line segments of length $|\mathbf{r}|$ (aligned along a considered direction) and measuring the probability to find the start of the line segments lying in phase (u) and the end lying in phase (v). The approach is based on the 3D-space described in a spherical coordinate system, by varying the polar angle θ from 0 to π and the azimuthal angle φ from 0 to 2π with increments of $\Delta\theta = \Delta\varphi = \pi/36$, see Fig. A.19. In order to represent an infinite domain, the unit cell is surrounded by its replica. A sampling template of positions (here 10,000) is used. Positions are equi-angularly spaced at distance $|\mathbf{r}|$ from a random central point, see Fig. A.19.

Fig. A.20 (a) reports $S_2^{I,I}$, $S_2^{M,M}$, $S_2^{I,M} = S_2^{M,I}$ distributions along the three reference axis of the unit cell (30 inclusions and $c = 0.25$). Main signatures of a homogeneous medium are retrieved as the two point probability functions satisfy Eq. (A.1) for $|\mathbf{r}|/L \to 0$ and for $|\mathbf{r}|/L \to 1$. Probability functions are shown to be damped, oscillating functions about their long-range asymptotic values c^2, $(1-c)^2$, $c(1-c)$ when $|\mathbf{r}|/L \to 1$. This is the consequence of the impenetrability condition defined here since a minimum distance between neighboring spheres centers of 2.07 times the inclusion radius is considered (Smith and Torquato, 1988). Note that in the case of fully penetrable particles, two-point probability functions would be expected to exponentially decays without oscillations.

Figs. A.20 (b–d) show maps of two-point probability functions for fixed values of $|\mathbf{r}|$ in the 3D-space and illustrate the statistical isotropy of the RVE. One can note that for a given $|\mathbf{r}|/L$, the value of the probability functions is relatively constant, indicating that the response is independent of the direction of the vector $\mathbf{r}$.

From this analysis, it can be reasonably assumed that the adopted RVE may be considered as statistically homogeneous and isotropic.

Appendix B. Heterogeneity at the inclusion scale

Let us denote by N_i the number of spherical inclusions in the RVE. At each time of the deformation process, the average strain tensor in each single inclusion $I = 1 \ldots N_i$ is obtained from the relationship:

$$\bar{\boldsymbol{\varepsilon}}_I(t) = \frac{1}{V_I(t)} \int_{V_I(t)} \boldsymbol{\varepsilon}(t)\, \mathrm{d}v, \tag{B.1}$$

where $\boldsymbol{\varepsilon}(t)$ is the strain in the volume element $\mathrm{d}v$ and $V_I(t)$ is the volume of inclusion I at time t. Based on the discretization of the RVE by finite elements, the strain tensor $\boldsymbol{\varepsilon}(t)$ in Eq. (B.1) is approximated at the centroid of the tetrahedron finite element belonging to the spherical inclusion I. The mean strain tensor in inclusion I is then expressed, in its discretized form, by:

$$\bar{\boldsymbol{\varepsilon}}_I(t) = \frac{\sum_{p=1}^{N_I} \boldsymbol{\varepsilon}_p(t)\, \mathrm{d}v_p(t)}{\sum_{p=1}^{N_I} \mathrm{d}v_p(t)}, \tag{B.2}$$

where N_I is the number of finite elements belonging to inclusion I, $\boldsymbol{\varepsilon}_p(t)$ is the strain tensor inside the finite element p belonging to inclusion I and $\mathrm{d}v_p(t)$ its volume. Note that the overall strain tensor in the inclusion phase $\bar{\boldsymbol{\varepsilon}}_i(t)$ can be derived from Eq. (B.1):

$$\bar{\boldsymbol{\varepsilon}}_i(t) = \frac{1}{V_i(t)} \int_{V_i(t)} \boldsymbol{\varepsilon}(t)\, \mathrm{d}v = \frac{\sum_{I=1}^{N_i} \bar{\boldsymbol{\varepsilon}}_I(t) V_I(t)}{\sum_{I=1}^{N_i} V_I(t)}. \tag{B.3}$$

In Eq. (B.3), $V_i(t)$ is the volume of the inclusion phase at time t. The mean stress tensor in each inclusion and the overall stress tensor in

the inclusion phase can be obtained by replacing $\boldsymbol{\varepsilon}$ by $\boldsymbol{\sigma}$ in Eqs. (B.1)–(B.3).

Appendix C. Heterogeneity at the finite element scale

At each time t of the deformation process, the minimum $\varepsilon_{\min}(t)$ and maximum $\varepsilon_{\max}(t)$ values of the uniaxial strain in the inclusion domain are captured. For sake of brevity, the label t referring to time is omitted in this Appendix. To analyze the strain heterogeneity in the inclusion phase, the probability density function Π_ε defined on the interval $[\varepsilon_{\min}, \varepsilon_{\max}]$ is introduced such that:

$$\Pi_\varepsilon(\varepsilon) \geqslant 0, \ \forall \varepsilon \in [\varepsilon_{\min}, \varepsilon_{\max}] \qquad \int_{\varepsilon_{\min}}^{\varepsilon_{\max}} \Pi_\varepsilon(\varepsilon)\, \mathrm{d}\varepsilon = 1. \tag{C.1}$$

The probability of finding a strain lying inside the interval $[\varepsilon_1, \varepsilon_2]$ is given by:

$$P_\varepsilon(\varepsilon_1 \leqslant \varepsilon \leqslant \varepsilon_2) = \int_{\varepsilon_1}^{\varepsilon_2} \Pi_\varepsilon(\varepsilon)\, \mathrm{d}\varepsilon. \tag{C.2}$$

In the analysis, the interval $[\varepsilon_{\min}, \varepsilon_{\max}]$ is divided into an odd number I_ε of subintervals of length $L_\varepsilon = [\varepsilon_{\max} - \varepsilon_{\min}]/I_\varepsilon$. The kth interval $\text{Int}_\varepsilon(k)$:

$$\text{Int}_\varepsilon(k) = [\varepsilon_{1k}, \varepsilon_{2k}] \qquad \varepsilon_{1k} = \varepsilon_{\min} + L_\varepsilon(k-1) \qquad \varepsilon_{2k} = \varepsilon_{\min} + L_\varepsilon k \tag{C.3}$$

is centered around the strain value:

$$\varepsilon_k = \varepsilon_{\min} + L_\varepsilon\left(k - \frac{1}{2}\right). \tag{C.4}$$

The family $F_{\varepsilon k}$ is defined as being the group of finite elements with uniaxial strain ε belonging to the interval $\text{Int}_\varepsilon(k)$:

$$F_{\varepsilon k} = \{\text{Finite elements with uniaxial strain } \varepsilon \in \text{Int}_\varepsilon(k)\}. \tag{C.5}$$

We consider the strain ε_k, given by Eq. (C.4), as a measure of the uniaxial strain of all finite elements of family $F_{\varepsilon k}$. In addition, $F_{\varepsilon k}$ is characterized by the appearance frequency $P_{\varepsilon k}$ of ε_k, which can also be seen as the probability for a finite element to belong to the family $F_{\varepsilon k}$. According to the adopted discretization scheme, and assuming that the probability density function Π_ε is piecewise constant, one has:

$$P_{\varepsilon k} = P_\varepsilon(\varepsilon_{1k} \leqslant \varepsilon_k \leqslant \varepsilon_{2k}) = L_\varepsilon \Pi_\varepsilon(\varepsilon_k). \tag{C.6}$$

Let us denote by N the total number of finite elements in the inclusion domain, and by N_k the corresponding number of elements in $F_{\varepsilon k}$, then the appearance frequency is expressed as:

$$P_{\varepsilon k} = \frac{\sum_{j=1}^{N_k} \mathrm{d}v_j}{\sum_{j=1}^{N} \mathrm{d}v_j}, \tag{C.7}$$

where $\mathrm{d}v_j$ represents the volume of the finite element j. A combination of Eqs. (C.6) and (C.7) allows one to identify the probability density function Π_ε. Similar approach is adopted to define the probability density function Π_σ describing the stress distribution within the inclusion domain, substituting ε by σ in Eqs. (C.1) to (C.7) and using $L_\sigma = [\sigma_{\max} - \sigma_{\min}]/I_\sigma$.

In the present work, we have adopted $I_\varepsilon = I_\sigma = 51$.

References

Berbenni, S., Favier, V., Lemoine, X., Berveiller, M., 2004. Micromechanical modeling of the elastic–viscoplastic behavior of polycrystalline steels having different microstructures. Mater. Sci. Eng. A 372, 128–136.

Berveiller, M., Zaoui, A., 1979. An extension of the self-consistent scheme to the plastically flowing polycrystals. J. Mech. Phys. Solids 26, 325.

Bornert, M., 2001. Homogeneisation des milieux aleatoires; bones et estimations. In: Bornert, M., Bretheau, T., Gilormini, P. (Eds.), Homogeneisation en Mecanique des Materiaux. Hermes Science Publication.

Bornert, M., Masson, R., Ponte Castañeda, P., Zaoui, A., 2001. Second-order estimates for the effective behaviour of viscoplastic polycrystalline materials. J. Mech. Phys. Solids 49, 2737–2764.

Brenner, R., Suquet, P., 2013. Overall response of viscoelastic composites and polycrystals: exact asymptotic relations and approximate estimates. Int. J. Solids Struct. 50, 1824–1838.

Brinson, I.C., Lin, W.S., 1998. Comparison of micromechanics methods for effective properties of multiphase viscoelastic composites. Compos. Struct. 41, 353–367.

Chaboche, J.L., Kanoute, P., Roos, A., 2005. On the capabilities of mean-field approaches for the description of plasticity in metal-matrix composites. Int. J. Plast. 21, 1409–1434.

Christensen, R.M., 1969. Viscoelastic properties of heterogeneous media. J. Mech. Phys. Solids 17, 23–41.

Coulibaly, M., Sabar, H., 2011. New integral formulation and self-consistent modeling of elastic–viscoplastic heterogeneous materials. Int. J. Solids Struct. 48, 753–763.

De Botton, G., Tevet-Deree, L., 2004. The response of a fiber-reinforced composite with a viscoelastic matrix phase. J. Compos. Mater. 38, 1255–1277.

Doghri, I., Adam, L., Bilger, N., 2010. Mean-field homogenization of elasto-viscoplastic composites based on a general incrementally affine linearization method. Int. J. Plast. 26, 219–238.

Doghri, I., Ouaar, A., 2003. Homogenization of two-phase elasto-plastic composite materials and structures. Study of tangent operators, cyclic plasticity and numerical algorithms. Int. J. Solids Struct. 40, 1681–1712.

Eshelby, J.D., 1957. The determination of the elastic field of an ellipsoidal inclusion, and related problems. Proc. R. Soc. A 241, 376–396.

Forte, S., Vianello, M., 1996. Symmetry classes for elasticity tensors. J. Elast. 43, 81–108.

Hashin, Z., 1969. The inelastic inclusion problem. Int. J. Eng. Sci. 7, 11–36.

Hill, R., 1965. Continuum micro-mechanics of elastoplastic polycrystals. J. Mech. Phys. Solids 13, 89–101.

Hutchinson, J.W., 1976. Bounds and self-consistent estimates for creep of polycrystalline materials. Proc. R. Soc. London A 348, 101–127.

Kiryk, R., Petryk, H., 1998. A self-consistent model of rate dependent plasticity of polycrystals. Arch. Mech. 50, 247–263.

Koplik, J., Needleman, A., 1988. Void growth and coalescence in porous plastic solids. Int. J. Solids Struct. 24, 835–853.

Kouddane, R., Molinari, A., Canova, G.R., 1993. In: Proceedings of the International Seminar MECAMAT'91, Fontenblau/France/7-8 August 1991. A.A.Balkema, Ch. Self-consistent Modelling of Heterogeneous Viscoelastic and Elastoviscoplastic Materials, pp. 129–141.

Kowalczyk-Gajewska, K., 2012. Estimation of overall properties of random polycrystals with the use of invariant decompositions of Hooke's tensor. Int. J. Solids Struct. 49, 3022–3037.

Kowalczyk-Gajewska, K., Petryk, H., 2011. Sequential linearization method for viscous/elastic heterogeneous materials. Eur. J. Mech. Solids/A 30, 650–664.

Kröner, E., 1958. Berechung der elastischen konstanten des vielkristalls aus den konstanten des einkristalls. Z. Phys. A 151, 504–518.

Lahellec, N., Suquet, P., 2007. On the effective behavior of nonlinear inelastic composites: I. incremental variational principles. J. Mech. Phys. Solids 55, 1932–1963.

Lahellec, N., Suquet, P., 2013. Effective response and field statistics in elasto-plastic and elasto-viscoplastic composites under radial and non-radial loadings. Int. J. Plast. 42, 1–30.

Laws, N., McLaughlin, R., 1978. Self-consistent estimates for viscoelastic creep compliance of composite materials. Proc. R. Soc. London A359, 251–273.

Lebensohn, R.A., Liu, Y., Ponte Castañeda, P., 2004. On the accuracy of the self-consistent approximation for polycrystals: comparison with full-field numerical simulations. Acta Mater. 52, 5347–5361.

Lebensohn, R.A., Tomé, C.N., 1993. A self-consistent anisotropic approach for the simulation of plastic deformation and texture development of polycrystals: application to zirconium alloys. Acta Metall. Mater. 41, 2611–2624.

Li, J., Weng, G.J., 1994. Strain-rate sensitivity, relaxation behavior and complex moduli of a class of isotropic viscoplastic composites. J. Eng. Mater. Technol. 116, 495–504.

Mareau, C., Berbenni, S., 2015. An affine formulation for the self-consistent modelling of elasto-viscoplastic heterogeneous materials based on the translated field method. Int. J. Plast. 64, 134–150.

Masson, R., Bornert, M., Suquet, P., Zaoui, A., 2000. An affine formulation for the prediction of the effective properties of non-linear composites and polycrystals. J. Mech. Phys. Solids 48, 1203–1227.

Masson, R., Zaoui, A., 1999. Self-consistent estimates of the rate-dependent elasto-plastic behaviour of polycrystalline materials. J. Mech. Phys. Solids 47, 1543–1568.

Mercier, S., Jacques, N., Molinari, A., 2005. Validation of an interaction law for the Eshelby inclusion problem in elasto-viscoplasticity. Int. J. Solids Struct. 42, 1923–1941.

Mercier, S., Molinari, A., 2009. Homogenization of elastic–viscoplastic heterogeneous materials: self-consistent and Mori–Tanaka schemes. Int. J. Plast. 25, 1024–1048.

Mercier, S., Molinari, A., Berbenni, S., Berveiller, M., 2012. Comparison of different homogenization approaches for elastic–viscoplastic materials. Model. Simul. Mater. Sci. Eng. 20, 024044.

Molinari, A., 2002. Averaging models for heterogeneous viscoplastic and elastic viscoplastic materials. J. Eng. Mater. Technol. Trans. ASME 124, 62–70.

Molinari, A., Ahzi, S., Kouddane, R., 1997. On the self-consistent modeling of elastic-plastic behavior of polycrystals. Mech. Mater. 26, 43–62.

Molinari, A., Canova, G.R., Ahzi, S., 1987. Self-consistent approach of the large deformation polycrystal visco-plasticity. Acta Metall. 35, 2983–2994.

Molinari, A., El Houdaigui, F., Toth, L.S., 2004. Validation of the tangent formulation for the solution of the non-linear Eshelby inclusion problem. Int. J. Plast. 20, 291–307.

Molinari, A., Toth, L.S., 1994. Tunning a self-consistent viscoplastic model by finite element results I: modelling. Acta Metall. Mater. 42, 2453–2458.

Mori, T., Tanaka, K., 1973. Average stress in matrix and average elastic energy of materials with misfitting inclusions. Acta Metall. 21, 571–574.

Moulinec, H., Suquet, P., 2003. Intraphase strain heterogeneity in nonlinear composites: a computational approach. Eur. J. Mech. Solids/A 22, 751–770.

Paquin, A., Sabar, H., Berveiller, M., 1999. Integral formulation and self-consistent modelling of elastoviscoplastic behavior of heterogeneous materials. Arch. Appl. Mech. 69, 14–35.

Perzyna, P., 1986. Internal state variable description of dynamic fracture of ductile solids. Int. J. Solids Struct. 22, 797–818.

Pichler, C., Lackner, R., 2009. Upscaling of viscoelastic properties of highly-filled composites: investigation of matrix inclusion- type morphologies with power-law viscoelastic material response. Compos. Sci. Technol. 69, 2410–2420.

Pierard, O., Doghri, I., 2006. An enhanced affine formulation and the corresponding numerical algorithms for the mean-field homogenization of elasto-viscoplastic composites. Int. J. Plast. 22, 131–157.

Pierard, O., González, C., Segurado, J., LLorca, J., Doghri, I., 2007. Micromechanics of elasto-plastic materials reinforced with ellipsoidal inclusions. Int. J. Solids Struct. 44, 6945–6962.

Pierard, O., LLorca, J., Segurado, J., Doghri, I., 2007. Micromechanics of particle-reinforced elasto-viscoplastic composites: finite element simulations versus affine homogenization. Int. J. Plast. 23, 1041–1060.

Ponte Castañeda, P., 1992. New variational principles in plasticity and their application to composite materials. J. Mech. Phys. Solids 40, 1757–1788.

Ricaud, J.-M., Masson, R., 2009. Effective properties of linear viscoelastic heterogeneous media: Internal variables formulation and extension to ageing behaviours. Int. J. Solids Struct. 46, 1599–1606.

Rougier, Y., Stolz, C., Zaoui, A., 1993. Representation spectrale en viscoèlasticité linéaire de matériaux hétérogènes. C. R. Acad. Sci. Paris 316, 1517–1522, Serie II.

Rougier, Y., Stolz, C., Zaoui, A., 1994. Self-consistent modelling of elastic–viscoplastic polycrystals. C.R. Acad. Sci. Paris 318, 145–151, Serie II.

Sabar, H., Berveiller, M., Favier, V., Berbenni, S., 2002. A new class of micro-micro models for elastic–viscoplastic heterogeneous materials. Int. J. Solids Struct. 39, 3257–3276.

Smith, P., Torquato, S., 1988. Computer simulation results for the two-point probability function of composite media. J. Comput. Physics 76, 176–191.

Suquet, P., 1985. Homogenization techniques for composite media. Elements of Homogenization for Inelastic Solid Mechanics. Springer-Verlag, Berlin, Ch., pp. 193–278.

Torquato, S., 2002. Random Heterogeneous Materials. Microstructure and Macroscopic Properties. Springer.

Turner, P.A., Tomé, C.N., 1994. Self-consistent modeling of visco-elastic polycrystals: application to irradiation creep and growth. J. Mech. Phys. Solids 41, 1191–1211.

Wang, H., Wu, P.D., Tomé, C.N., Huang, Y., 2010. A finite strain elastic–viscoplastic self-consistent model for polycrystalline materials. J. Mech. Phys. Solids 58, 594–612.